Phosphorus sources for phosphatic Cambrian carbonates

P sources for phosphatic Cambrian carbonates

Jessica R. Creveling[1*], David T. Johnston[1†], Simon W. Poulton[2], Benjamin Kotrc[1], Christian März[3], Daniel P. Schrag[1], Andrew H. Knoll[1,4]

[1] *Department of Earth and Planetary Sciences, Harvard University, 20 Oxford Street, Cambridge, MA 02138, USA*

[2] *School of Earth and Environment, University of Leeds, Leeds, LS2 9JT, UK*

[3] *School of Civil Engineering and Geosciences, Newcastle University, Drummond Building, Newcastle upon Tyne, NE1 7RU, UK*

[4] *Department of Organismic and Evolutionary Biology, Harvard University, 26 Oxford Street, Cambridge, MA 02138, USA*

[*]Email: jcrevel@gps.caltech.edu

[†]Email: *johnston@eps.harvard.edu*

ABSTRACT

The fossilization of organic remains and shell material by calcium phosphate minerals provides an illuminating, but time-bounded, window into Ediacaran—Cambrian animal evolution. For reasons that remain unknown, phosphatic fossil preservation declined significantly through Cambrian Series 2. Here we investigate the phosphorus (P) sources for phosphatic Cambrian carbonates, presenting sedimentological, petrographic, and geochemical data from the Cambrian Series 2–3 Thorntonia Limestone, Australia, some of the youngest Cambrian strata to display exceptional phosphatic preservation of small shelly fossils. We find that within Thorntonia sediments, phosphate was remobilized by organic decay and bacterial iron reduction, with subsequent reprecipitation largely as apatite within the interiors of small shelly fossils. We discuss the merits of bioclastic-derived, organic matter-bound, or iron-bound P as potential sources to these strata. Petrographic observations suggest that the dissolution of phosphatic skeletal material did not source P for fossil preservation. In contrast, high organic carbon contents imply significant organic fluxes of P to Thorntonia sediments. Sedimentology and iron-speciation data indicate that phosphorus enrichment occurred during times of expanded anoxic, ferruginous conditions in subsurface water masses, suggesting that phosphorus adsorption to iron minerals precipitating from the water column provided a second significant P source to Thorntonia sediments. Simple

stoichiometric models suggest that by themselves neither organic carbon burial nor an iron shuttle can account for the observed phosphorus enrichment. Thus, we infer that both processes were necessary for the observed phosphorus enrichment and subsequent fossil preservation in the Thorntonia Limestone.

INTRODUCTION

Phosphorite and phosphatic carbonate define a spectrum of sedimentary lithologies enriched in the authigenic calcium phosphate mineral apatite (Kazakov, 1937; Baturin and Bezrukov, 1979; Riggs, 1986; Cook and Shergold, 1986; Cook et al., 1990; Föllmi, 1996; Trappe, 2001). The punctuated temporal distribution (Cook and McElhinny, 1979; Cook and Shergold, 1984, 1986) and evolving spatial distribution (Brasier and Callow, 2007) of phosphatic lithologies through Earth history suggest that unique and restrictive physical (Filippelli and Delaney, 1992) and/or chemical (e.g., Föllmi, 1996) conditions govern phosphate deposition in time and space.

There are many reasons to want to understand this distribution. Perhaps foremost is the practical concern for understanding how ore-grade sedimentary phosphorites form (e.g., Cook and Shergold, 1986). As with petroleum, phosphate ores are approaching peak production, while global demand continues to rise (Cordell et al., 2009; Filippelli, 2011). At the same time, biogeochemists increasingly invoke perturbations to the ancient phosphorus cycle to explain inferred fluctuations in biological productivity, organic carbon burial and oxidant accumulation over geological time-scales (Tyrrell, 1999; Bjerrum and Canfield, 2002; Saltzman, 2005; Holland et al., 2006; Konhauser et al., 2007; Algeo and Ingall, 2007; Planavsky et al., 2010; Swanson-Hysell et al., 2012). Finally, phosphatic deposits provide a direct window into evolutionary history through

58 the exceptional preservation of fossils (Cook, 1992; Bengtson and Zhao, 1997; Xiao and
59 Knoll, 2000; Butterfield, 2003; Porter, 2004a).
60 A global phosphogenic window coincides with major evolutionary innovation
61 during the Ediacaran and Cambrian periods (Cook and Shergold, 1984; 1986; Cook,
62 1992). Much of our knowledge of early animal diversification derives from
63 biomineralized and soft-bodied metazoans replaced and/or templated by phosphate
64 minerals (Bengtson et al., 1990; Xiao and Knoll, 1999; 2000; Donoghue et al., 2006;
65 Dornbos et al., 2006; Kouchinsky et al., 2012). Phosphatization taphonomy is tied to the
66 biogeochemical cycle of phosphorus and, for reasons that remain unknown, a major
67 decline in the incidence of phosphatic lithologies and phosphatic fossil preservation
68 occurs during Cambrian Series 2 (Cook and McElhinny, 1979; Porter, 2004b; Donoghue
69 et al., 2006). To understand the loss of phosphatic lithologies, and the consequent closure
70 of the Cambrian phosphatization taphonomic window, we must first understand how
71 phosphorus entered the sediment column and how it was subsequently redistributed and
72 concentrated around skeletal elements. In this paper, we ask specifically: what was the
73 source of phosphorus to phosphatic carbonates characterized by exceptional skeletal
74 preservation?
75 Geochemistry provides one avenue to address this question. A common view
76 holds that enhanced delivery of reactive phosphorus (i.e., phosphorus that may undergo
77 biogeochemical transformations within the sediment column) to the sea floor is the
78 primary variable governing the development of phosphatic lithologies (e.g., see Föllmi,
79 1996, and references therein; Papineau, 2010). In modern marine environments, the
80 delivery of reactive phosphorus to the sea floor occurs predominantly in association with

two phases (e.g., Delaney, 1998; Benitez-Nelson, 2000): phosphorus bound within organic matter (Redfield, 1958) and/or phosphorus adsorbed to/co-precipitated with particulate iron minerals (herein referred to as the 'Fe-P shuttle') (Berner, 1973; Shaffer, 1986; Feely et al., 1991; Feely et al., 1998; Poulton and Canfield, 2006). To examine the extent to which these reactive phosphorus sources contributed to ancient phosphatic deposits, we report high-resolution phosphorus and iron speciation data, stable carbon isotope measurements, and trace element concentrations for the phosphatic Thorntonia Limestone, Georgina Basin, Australia (Cambrian Series 2–3; Southgate, 1988; Southgate and Shergold, 1991), and, for comparison, the overlying non-phosphatic Arthur Creek Formation. We explore the possibility that bioclastic-bound, organic-bound, and iron-bound P sourced the Thorntonia phosphatic carbonates and develop simple mathematical models to assess the relative importance of organic- and iron-bound P. We find that while the high organic carbon content of the Thorntonia Limestone suggests that organic-bound P contributed significantly to authigenic apatite formation, C to P ratios indicate that organic-bound P was insufficient to account entirely for the observed phosphorus enrichment. Sedimentology and iron speciation data indicate that these formations accumulated under anoxic, ferruginous subsurface water masses, allowing for the possibility that P adsorbed to iron minerals precipitating from the water column augmented organic-bound P delivery to the sediment column. Nonetheless, simple mathematical models indicate that, by itself, iron-bound phosphorus delivery is also incapable of accounting for the observed phosphorus enrichment. Thus, we infer that both organic-bound and iron-bound phosphorus sources were necessary for the development of the fossil-bearing phosphatic carbonates of the Thorntonia Limestone.

GEOLOGIC BACKGROUND

The Centralian Superbasin is a laterally extensive intracratonic basin that initiated during Neoproterozoic transcontinental rifting of Rodinia. Regional tectonic events subsequently dissected the superbasin into a mosaic of discrete, asymmetric, polyphase foreland basins (Fig. 1a; Walter et al, 1995; Lindsay, 2002; Dunster et al., 2007). Here, we focus on the phosphatic Cambrian strata of the southern Georgina Basin (Cook and Shergold, 1986; Southgate, 1988; Southgate and Shergold, 1991), which deposited variably and diachronously across the basin (Cook and Shergold, 1986; Southgate, 1988; Howard, 1990; Southgate and Shergold, 1991; Dunster et al., 2007).

The Narpa Group encompasses Cambrian Series 2 and Series 3 stratigraphy of the southern Georgina Basin (Fig. 1b; Ambrose et al., 2001; Dunster et al., 2007). Deposition of its lowermost member, the phosphatic Thorntonia Limestone, reflects a major transgression and expansion of the Georgina Basin. For this reason, the basal contact of the Thorntonia Limestone can unconformably overlie the Shadow Group, conformably and gradationally overlie the Shadow Group, or overlie and re-work crystalline basement (Fig. 1b). The rest of the Narpa Group records a basin-wide, shallowing-upward succession that transitions from outer (lower Arthur Creek Formation), middle (upper Arthur Creek Formation) and inner ramp (Steamboat Sandstone) depositional environments into a flat-topped carbonate platform (Arrinthrunga Formation; Ambrose et al., 2001; Dunster et al., 2007).

Trilobite biostratigraphy assigns Thorntonia rocks to the Ordian and early Templetonian stages of Australian chronostratigraphy (Laurie, 2004a,b; Dunster et al.,

2007), correlative to Cambrian Series 2, Stage 4 and, possibly, lowermost Series 3, Stage 5 (Fig. 1b; Babcock and Peng, 2007; Peng and Babcock, 2011). Trilobite biozones within the Arthur Creek Formation are diagnostic for the Australian regional Ordian–Boomerangian stages (Laurie, 2004a, b; Dunster et al., 2007), correlative to uppermost Stage 4 of Cambrian Series 2 through to the Guzhangian Stage of Cambrian Series 3 (Fig. 1b; Babcock and Peng, 2007; Peng and Babcock, 2011).

METHODS

We examined the sedimentology and lithofacies associations of the Thorntonia and Arthur Creek formations within drill core NTGS 99/1 reposited at the Northern Territory Geological Survey, Alice Springs, Australia. With a water-cooled saw, we cut 534 three-cm-long, quarter-core samples perpendicular to bedding at ~10-25 cm resolution between 597.58 and 347.98 meters core depth (mcd). Each sample was again divided (perpendicular to bedding) into two subsamples, one half designated as a hand-sample or thin-section billet, the other half pulverized with a steel ring mill. Each hand-sample billet was micro-drilled along individual laminations for carbonate carbon ($\delta^{13}C_{carb}$) and carbonate oxygen ($\delta^{18}O_{carb}$) isotopic analysis. The evolved CO_2 was measured against an in-house reference gas on a VG Optima dual-inlet mass spectrometer attached to a VG Isocarb preparation system. We report isotopic values in the V-PDB per mil (‰) notation. Standard reproducibility was $1\sigma = < 0.1$‰ and 0.2‰ for $\delta^{13}C_{carb}$ and $\delta^{18}O_{carb}$, respectively.

Sample powders were divided for carbon, phosphorus, iron, and trace element geochemical analyses aimed at diagnosing the sediment- and water-column geochemistry

150 at the time of phosphatic carbonate deposition. To determine carbon mass fractions, we
151 acidified 5-10 g of powdered sample with cold, 2.5 M hydrochloric acid. The resulting
152 insoluble residue (i.e., the non-carbonate fraction, comprised predominately of
153 siliciclastics and organic matter) was isolated by filtration, rinsed thoroughly with de-
154 ionized water, then dried and weighed. The total carbonate fraction was estimated as the
155 weight percent difference between the bulk sample and the insoluble residue. To
156 determine the weight percent of total organic carbon (TOC) and its isotopic composition
157 ($\delta^{13}C_{org}$), aliquots of the insoluble residue were combusted within a Carlo Erba NA 1500
158 Analyzer attached to a Thermo Scientific Delta V Advantage isotope ratio mass
159 spectrometer. Reproducibility of $\delta^{13}C_{org}$ for an acetanilide standard was 0.16‰ (1σ). Of
160 the 100 samples processed, 29 were analyzed in duplicate and yielded an analytical
161 reproducibility of 1σ = 0.07 weight percent (wt.%) TOC. Finally, we estimated the wt.%
162 of silicate phases (either clastic or authigenic) as the wt.% of the insoluble fraction minus
163 the wt.% of the TOC fraction.
164 The speciation of phosphorus (P) was determined with a modified sequential
165 extraction methodology for marine sediment (Ruttenberg, 1992). Here, 150-200 mg of
166 rock powder was sequentially extracted with 10 mL each of (1) 0.3 M sodium-citrate/1 M
167 sodium bicarbonate/0.14 M sodium dithionite (pH = 7.5) for P bound to
168 reducible/reactive ferric iron minerals (P_{Fe}), (2) 1 M sodium acetate (pH = 4.0) for
169 carbonate fluorapatite, biogenic hydroxyapatite, and carbonate-bound P ($P_{auth+carb}$), (3) 1.2
170 M cold HCl for crystalline fluorapatite (P_{xl}), and (4) 1.2 M cold HCl after a 2 hour
171 ignition at 550°C for organic P (P_{org}). To prevent P readsorption during the first two
172 extraction steps, two 5 mL 1 M $MgCl_2$ washes were performed post-extraction.

Phosphorus in extracts and wash solutions (except P_{Fe}) was analyzed spectrophotometrically (Thermo Genesys 6) by the molybdate-blue method (Strickland and Parsons, 1972; Ruttenberg, 1992); P_{Fe} was measured by inductively coupled plasma optical emission spectrometry (ICP-OES; Varian Vista-MPX). We note that Ruttenberg (1992) ascribes P-speciation phase (3), P_{xl}, to detrital fluorapatite of igneous and metamorphic origin. We abbreviate this phase as 'xl' for 'crystalline' so as to remove reference to a genetic mechanism (i.e., detrital) for an operationally-defined phase based on a chemical extraction procedure. We hypothesize about the origin of this phase in greater detail in the discussion.

To verify the efficiency of the sequential extraction method, total P (P_T) values were determined independently (SGS Mineral Services Group) by inductively coupled plasma atomic emissions spectrometry (ICP-AES) after a standard four acid digestion ($HF\text{-}HClO_4\text{-}HCl\text{-}HNO_3$). These analyses also provide the additional major and trace metal concentrations reported below. To account for variable dilution by siliciclastic influx, we report element concentrations normalized to aluminum (Al) in wt.%/wt.% and ppm/wt.% units for major and trace elements, respectively.

To determine the speciation of iron within our samples, we applied a modified version of the sequential extraction method of Poulton and Canfield (2005). Here, 80-100 mg of rock powder was sequentially extracted with 10 mL each of (1) 1 M sodium-acetate, adjusted to pH 4.5 with acetic acid to extract Fe associated with carbonate phases such as siderite and ankerite (Fe_{carb}); (2) 0.28 M sodium dithionite, adjusted to pH 4.8 with 0.2 M acetic acid/0.25 M tri-sodium citrate, for iron oxides such as hematite and goethite (Fe_{ox}); and (3) 0.2 M ammonium oxalate/0.17 M oxalic acid for magnetite

(Fe_{mag}). The boiling chromium reduction distillation of Canfield et al. (1986) was used to quantify sulfur (S) within pyrite from the insoluble residues derived from carbonate dissolution. We used a pyrite stoichiometry (FeS_2) to relate the extracted S back to iron (Fe_{py}). Total Fe (Fe_T), which comprises the sum of the diagenetically highly reactive phases ($Fe_{HR} = Fe_{carb} + Fe_{ox} + Fe_{mag} + Fe_{py}$), as well as unreactive Fe (Fe_U; predominately silicate-bound Fe), was determined via a boiling HF-HNO_3-$HClO_4$ extraction on an additional aliquot of sample powder. All iron concentrations were measured by atomic absorption spectrometry (AAS). Eight replicates of one sample, 572.64 mcd, yield a RSD of 2%, 13%, and 71% for Fe_{carb}, Fe_{ox}, and Fe_{mag}, respectively. The high RSD of the latter two phases result from measured quantities close to the instrument detection limit; that is, the average wt.% ± 1σ for the eight Fe-speciation replicates is 0.110±0.002, 0.016±0.002, and 0.001±0.001 for Fe_{carb}, Fe_{ox}, and Fe_{mag}, respectively. At higher Fe concentrations for each fraction, the RSD is <5% for each stage, and this is also the case for Fe_{py} and Fe_T (Poulton and Canfield, 2005).

RESULTS

Lithofacies descriptions and paleoenvironmental interpretations for the Thorntonia Limestone and Arthur Creek Formation from drill core NTGS 99/1

Markings on drill core NTGS 99/1 assign 598.4–580.1 mcd, 580.1–558.7 mcd, and 558.7–554.7 mcd to the informal lower, middle, and upper members, respectively, of the Thorntonia Limestone (previously Hay River Formation), and 554.7–103.2 mcd to the Arthur Creek Formation (previously Marqua Formation; Ambrose et al., 2001; Dunster et al., 2007). In this study, we characterized the sedimentology and geochemistry of the

entire Thorntonia Limestone and the lowermost ~200 m of the lower Arthur Creek Formation.

Thorntonia Limestone

The Shadow Group is absent from NTGS 99/1. Here, the Thorntonia Limestone directly overlies Paleoproterozoic granite basement. The basal meters of the lower Thorntonia member include lithic fragments and sand grains within dolomudstone, with minor cubic pyrite crystals (Fig. 2a). More generally, the lower Thorntonia consists of dolomudstone and peloidal dolowackestone, with pervasive structural dissolution textures creating a stylolaminated to stylobedded fabric (Fig. 2b). Southgate and Shergold (1991) designated the basal, arkosic, terrigenous unit as a low-stand system tract, and the overlying stylolitic carbonate as a condensed transgressive / high-stand system tract.

Below 575.92 mcd (the lower Thorntonia Limestone) and from 580.1 - 575.92 mcd (the middle Thorntonia Limestone), the bulk lithology is dolostone. Stratigraphically above this horizon, up to the middle–upper Thorntonia Limestone contact at 558.7 mcd, the bulk lithology is limestone. Nevertheless, petrographic observation of the bulk limestone lithofacies above 575.92 mcd reveals rare euhedral dolomite rhombs within an otherwise calcimudstone or calciwackestone matrix.

The middle Thorntonia contains four interbedded and interlaminated lithofacies that occur within generally coarsening-upward meter- to sub-meter-scale packages (Fig. 2c). These lithofacies include: (1) black to medium gray carbonate mudstone; (2) dark to medium gray peloidal, bioclastic, and, occasionally, intraclastic wackestone; (3) medium to light gray peloidal and bioclastic packstone; and (4) medium to light gray bioclastic

grainstone. Carbonate mudstone or wackestone lithofacies define the base of each package and interlaminate or alternate gradationally on a centimeter to decimeter scale. These carbonate mud-dominated lithologies typically grade upward into, and contact sharply with, laminae and beds of packstone. When present, thin beds of bioclastic grainstone overlie packstone beds. These grainstone beds display basal erosional contacts with millimeter to half-centimeter-scale topography, and an upper contact that is either sharp or erosional and overlain by beds of black to medium-gray carbonate mudstone. In other cases, the upper contact is diffuse and conformable with beds of medium-gray packstone or wackestone (Fig. 2d). There is a broad up-core trend: packages initiate with progressively coarser lithologies and terminate with progressively thicker grainstone beds. The nature of deposition of the Thorntonia Limestone within NTGS 99/1 is consistent with the phosphatic lithofacies model from the northeast Georgina Basin (Cycle mP of Southgate, 1988). Southgate and Shergold (1991) assign these shallowing-upward cycles to the transgressive system tract.

We interpret the lithologic association of the middle Thorntonia to reflect deposition within a subtidal to intertidal depositional environment. Mudstone, wackestone, and packstone beds accumulated from suspension sedimentation in calm settings that lacked significant tidal, wave, or storm activity. The coarser grain size and subtle current-generated stratification observed in grainstone beds reflect a higher energy depositional environment. Grainstone beds reveal no internal grading, but do show evidence for amalgamation and winnowing of carbonate mud by currents or waves. Deposition under the influence of waves is also manifest in rosettes of brachiopod and trilobite shell fragments along basal scour surfaces of bioclastic grainstone beds (Fig. 2d).

Dunster et al. (2007) interpreted the black, carbonaceous carbonates of the Thorntonia Formation to represent deposition under dysoxic to anoxic conditions.

In NTGS 99/1, the upper Thorntonia encompasses a 4 meter-thick vuggy, fossiliferous dolopackstone with laminae, beds, and pockets of bioclastic dolograinstone (Fig. 2e). When present, dolospar crystals form a mosaic around bioclasts (primarily of lingulate brachiopods). In addition to representing a prominent matrix constituent, bioclasts occur as cumulate along dissolution seams.

Petrography of apatite distribution. Apatite displays three predominant modes within the middle and upper Thorntonia Limestone. First, within bioclast-rich carbonate lithologies, apatite occurs primarily as the internal molds (steinkerns) of conical small shelly fossils or, more commonly in the upper Thorntonia Limestone, as lingulate brachiopod skeletal debris (Fig. 3a). Apatite also occludes gaps between, and templates the exterior of, silica-replaced skeletons (Fig. 3a). Second, in rare instances, apatite occurs as cement within bioclastic grainstone lithologies (Fig. 3b), Third, within mud-supported, suspension-deposited carbonate, apatite occurs as sub-angular to sub-rounded coarse-silt to medium-sand-size grains, and as silt- to fine-sand-size, tabular or undulose grains within well-sorted, thin beds (Fig. 3c). Due to the textural maturity and fine grain-size of these lithologies, we cannot say conclusively whether these grains were eroded, transported and winnowed from a site of apatite authigenesis (i.e., allochthonous apatite grains) or whether they were sourced with a detrital siliciclastic influx. We favor the interpretation that these grains represent re-worked authigenic grains (i.e., intraclasts of authigenic cement and steinkern bioclasts) because we observe no comparable-size

287 detrital siliciclastic grains. Below, we discuss the origin of these grains in light of
288 geochemical data.
289
290 ***Arthur Creek Formation***
291 Within NTGS 99/1, the basal 10 m of the lower Arthur Creek encompasses a petroleum-
292 generating, massive black shale (Fig. 2e), or 'hot shale' (e.g., Dunster et al., 2007),
293 succeeded by planar, undulose, and corrugated interlaminae of black to dark gray organic
294 matter- and clay-rich shale and siltstone with medium to light gray calcimudstone and
295 dolomudstone. This shale also contains rare interbeds of very fine-grained bioclastic
296 packstone and grainstone (Fig. 2f). Clay- and iron-oxide-rich laminae include sub-
297 rounded to angular, very well sorted, monocrystalline quartz and authigenic pyrite
298 crystals, the latter of which often occlude pore space. Horizontal alignment of clay
299 minerals indicates that compaction enhanced the physical expression of lamination.
300 Commonly below ~490 mcd, and only rarely above, decimeter-scale light gray limestone
301 nodules displace surrounding laminations and retain faint remnants of lamination,
302 indicating nodular development during compaction, but before lithification (Fig. 2g). We
303 interpret individual laminae to reflect the gravitational settling of fine particles suspended
304 by dilute turbidity currents that wafted sediment towards the basin interior, consistent
305 with an outer-ramp depositional environment (Dunster et al., 2007). The fetid,
306 carbonaceous black shale and black, carbonaceous, laminated dolostone suggest
307 deposition under dysoxic to anoxic conditions (Dunster et al., 2007).
308 In the upper meters of the measured lower Arthur Creek, a second lithofacies
309 interbeds with the laminated facies (Fig. 2h). This facies includes interbeds of light gray

calcimudstone and siliciclastic siltstone. Rare truncation of undulatory laminae indicates intermittent deposition under the influence of currents. This facies is a harbinger of the more proximal, oxygenated ramp environment of the overlying upper Arthur Creek Formation (Dunster et al., 2007), which was not measured in this study. Southgate and Shergold (1991) assign the lower Arthur Creek to a transgressive system tract.

Geochemistry of the Thorntonia Limestone and Arthur Creek Formation

A generalized stratigraphic column of the Thorntonia and lower Arthur Creek is shown in Figure 4a alongside chemostratigraphic variation in $\delta^{13}C_{carb}$ (Fig. 4b), $\delta^{18}O_{carb}$ (Fig. 4c) and $\delta^{13}C_{org}$ (Fig. 4d). Cross-plots of $\delta^{13}C_{carb}$ and $\delta^{18}O_{carb}$ display no statistically significant co-variation (Fig. 4e), thereby suggesting that $\delta^{13}C_{carb}$ values, at least, represent the primary seawater isotopic composition. The $\delta^{13}C_{carb}$ curve generated for NTGS 99/1 displays two positive peaks, the first in the middle Thorntonia (563.92 mcd) and the second in the Arthur Creek (506.51 mcd). Consistent with trilobite biostratigraphy (Laurie, 2004a,b), we correlate the middle Thorntonia excursion to the Ordian–early Templetonian isotopic event and the Arthur Creek excursion to the Late Templetonian–Floran event (Fig. 4b; Lindsay et al., 2005). This assignment corroborates regional isotopic variation in the southern Georgina, Amadeus, and Daly Basins (Lindsay et al., 2005) and, further afield, to the Argentine Precordillera (Gomez et al., 2007), the Great Basin, U.S.A. (Saltzman, 2005), South China (Zhu et al., 2004; Guo et al., 2010), and northwest China (Wang et al., 2011).

Small magnitude discontinuities in $\delta^{13}C_{carb}$ chemostratigraphy occur across the informal member boundaries of the Thorntonia Limestone (Fig. 4b). These

discontinuities likely represent erosive events or hiatuses in deposition. In support of the former interpretation, an increase in Zr/Al occurs across the middle/upper Thorntonia contact (Supplementary Figure 1). Elevated Zr/Al ratios define erosional surfaces where high-energy currents winnow fine-grained, low-density siliciclastics (characterized by Al) and concentrate high-density minerals (characterized by Zr; Vine and Tourtelot, 1970). Unlike carbon isotopes, secondary fluid migration does not affect the Zr/Al ratio. Thus, this proxy confirms sediment winnowing during deposition of the upper Thorntonia. Regionally, the Thorntonia Limestone—Arthur Creek Formation contact represents a sequence boundary, with karstification developed along this surface in the western margin of the basin (Dunster et al., 2007). While the formation boundary within NTGS 99/1 represents a sharp lithologic break, $\delta^{13}C_{carb}$ values display general continuity across this boundary (Fig. 4b), suggesting either relative temporal continuity or fortuitous resumption of deposition with similar carbon isotopic composition. Isopach maps of the Arthur Creek show that the formation thickens to the east-southeast, where the NTGS 99/1 drill core intercepted the maximum depocenter of the preserved basin margin (Dunster et al., 2007). Thus, under the former scenario, the Thorntonia Limestone—Arthur Creek Formation boundary within NTGS 99/1 could represent a correlative conformity of the regional sequence boundary, with limited time missing across this lithologic contact.

Within NTGS 99/1, $\delta^{13}C_{org}$ displays co-variation with $\delta^{13}C_{carb}$ within the lower Thorntonia Limestone and no co-variation with $\delta^{13}C_{carb}$ within either the middle/upper Thorntonia or the Arthur Creek formations (Fig. 4d,f; lower Thorntonia: $R^2 = 0.75$; middle/upper Thorntonia: $R^2 = 0.04$; Arthur Creek: $R^2 = 0.2$). TOC varies from 0.1-2.9

356 wt.% in the Thorntonia, displaying a generally increasing trend in the lower Thorntonia
357 and high variance in the middle Thorntonia. TOC ranges from 0.1 to 2.5 wt.% in the
358 lower Arthur Creek, with higher values at the base of the formation, decreasing towards a
359 mean of 0.1 wt.% TOC in the upper 100 m of the measured core interval (Fig. 4d).
360 Despite the lack of covariance between $\delta^{13}C_{carb}$ and $\delta^{13}C_{org}$ in strata of the middle/upper
361 Thorntonia and the Arthur Creek Formation, one trend emerges: high (> 1.0 wt.%),
362 medium (0.2 < wt.% < 1.0), and low (< 0.2 wt. %) TOC correlate with light,
363 intermediate, and heavy $\delta^{13}C_{org}$ values (Fig. 4d). That is, the lightest $\delta^{13}C_{org}$ values occur
364 in the most organic- and phosphorus-rich lithofacies, the middle Thorntonia Limestone
365 (*cf*., Bartley et al., 1998, and Guo et al., 2013). The latter two TOC bins generally
366 correspond to samples from the Arthur Creek below and above ~430 mcd, respectively,
367 which is the transition between the laminated facies and the interbedded carbonate
368 mudstone–siliciclastic shale and siltstone facies.
369 Total phosphorus (P_T) within the Thorntonia Limestone ranges up to 3.9 wt.%
370 (Fig. 5a). P_T increases systematically within the lower Thorntonia and the lowermost
371 middle Thorntonia, followed by an additional increase around 575 mcd. We note that the
372 transition from dolostone (stratigraphically below 575.92 mcd) to limestone
373 (stratigraphically above 575.92 mcd) within drill core NTGS 99/1 occurs just below this
374 jump in P content (Figs 5a,b). The overlying meters of the middle and upper Thorntonia
375 display high variance in P_T. In contrast, the maximum value of P_T within the Arthur
376 Creek is 0.4 wt.%, but is typically much lower with a median of 0.03 wt.% and 1st and 3rd
377 quartile values of 0.02 and 0.04 wt.%, respectively (Fig. 5a).

We tested the fidelity of the P sequential extraction method by comparing the sum of the operationally-defined pools ($P_T = P_{xl} + P_{auth+carb} + P_{org} + P_{Fe}$) to the total phosphorus content determined by ICP-AES analysis. The consistency between these two measurement techniques (slope of linear regression = 1.1, $R^2 = 0.88$; Fig. 5e) increases confidence in the values of the constituent sequential extraction phases. In both the Thorntonia Limestone and the Arthur Creek Formation, the operationally-defined P_{xl} and $P_{auth+carb}$ phases dominate P_T, while P_{org} and P_{Fe} contribute a negligible fraction (Fig. 5b). The median (1^{st}, 3^{rd} quartile) percent contribution to P_T are: P_{xl} = 91.5% (77.5, 94.4), $P_{auth+carb}$ = 7.5% (3.7, 19.5), and P_{org} = 0.4% (0.2, 1.5). P_{Fe} was measured only on a subset of samples, but this phase contributes minimally to P_T (a median of 0.1% with 1^{st} and 3^{rd} quartiles of 0.0 and 0.4%, respectively).

Total iron (Fe_T) varies from 0.06-1.49 wt.% in the Thorntonia Limestone and from 0.32-2.71 wt.% in the Arthur Creek Formation (Fig. 5c). In general, Fe_T is lowest where P_T is highest. Based on the slope of linear regression, 88% of Fe_T resides in Fe_{HR} phases within the Thorntonia ($R^2 = 0.92$; Fig. 6a). In contrast, within the Arthur Creek, ~48% of Fe_T resides in Fe_{HR} ($R^2 = 0.57$; Fig. 6a), consistent with the higher siliciclastic fraction for these lithologies. The lower coefficient of determination for the Arthur Creek Formation reflects a decrease in Fe_{HR}/Fe_T from 0.66 at the base of the formation to ~0.3 near the top of the measured core interval. Reduced iron phases, Fe_{py} and Fe_{carb}, dominate Fe_{HR} in both formations, while oxidized and partially oxidized iron phases, Fe_{ox} and Fe_{mag}, contribute a minimal fraction (Fig. 5c). Based on the slope of the linear regression, 82% of Fe_{HR} resides as Fe_{carb} within the lower Thorntonia ($R^2 = 0.62$; Fig. 6c) while Fe_{py} accounts for only a minor contribution that has no statistically significant correlation with

401 Fe_{HR} (Fig. 6b). As such, the gradual decrease in Fe_{HR} within the lower Thorntonia reflects
402 a systematic decrease in Fe_{carb} from very high values of 1.3 wt.%, to ~0.3 wt.%. In the
403 middle and upper Thorntonia, 64% of Fe_{HR} resides as Fe_{py} (R^2 = 0.95; Fig. 6b) and 31%
404 resides as Fe_{carb} (R^2 = 0.82; Fig. 6c). For the lower Arthur Creek, ~73% and 26% of Fe_{HR}
405 reside in Fe_{py} (R^2 = 0.94; Fig. 6b) and Fe_{carb} (R^2 = 0.72; Fig. 6c), respectively.
406 When we parse the Fe-speciation data of the middle Thorntonia Limestone
407 samples by lithology, we see a similar partitioning of Fe phases as when we group all
408 samples within members (as presented above). Within the dolostone of the middle
409 Thorntonia (580.1 – 575.92 mcd), 98% of Fe_T resides in Fe_{HR} (R^2 = 0.99); in contrast,
410 within the limestone of the middle Thorntonia (575.92 mcd – 558.7 mcd), 89% of Fe_T
411 resides in Fe_{HR} (R^2 = 0.95). Likewise, within middle Thorntonia dolostone, 67% (R^2 =
412 0.94) and 27% (R^2 = 0.69) of Fe_{HR} resides in Fe_{py} and Fe_{carb}, respectively; within the
413 middle Thorntonia limestone, 68% (R^2 = 0.96) and 30% (R^2 = 0.86) of Fe_{HR} resides in
414 Fe_{py} and Fe_{carb}, respectively.
415 Within NTGS 99/1, the median (1^{st}, 3^{rd} quartile) percent acid insoluble fraction
416 (i.e., silicates) within the Thorntonia is 8.3% (5.3, 17.0) as compared to 44.0% (32.8,
417 54.3) for the Arthur Creek (Supplementary Figure 1). TOC/Al ratios are higher and more
418 variable in the Thorntonia than for the Arthur Creek (Supplementary Figure 1). Fe/Al
419 ratios and Mn/Al ratios decline throughout the lower Thorntonia (save for a couple of
420 high values in the upper Thorntonia; Supplementary Figure 1). The detrital-associated
421 trace element ratio Zr/Al is low and variable within the Thorntonia compared to the
422 Arthur Creek Formation and displays an abrupt increase across the middle/upper
423 Thorntonia boundary. (See Supplementary Information for a discussion of aluminum-

normalized concentrations of redox-sensitive and bioessential trace metals; Supplementary Figure 2.)

DISCUSSION

How do these geochemical data inform our understanding of the source of phosphorus to phosphatic Thorntonia carbonates and, more broadly, the loss of phosphatic lithologies and consequent closure of the phosphatization taphonomic mode during Cambrian Series 2? To address these questions, we combine petrographic observations with P-speciation data to quantify authigenic apatite within the Thorntonia Limestone. In turn, we explore the possibility that P bound within bioclasts, organic matter, or iron minerals sourced the observed P within these lithologies. Finally, we present a mathematical framework for which to deconvolve the relative contribution of the two most likely sources—P bound with organic matter or iron minerals—to authigenic apatite nucleation.

Source(s) of phosphorus to the Thorntonia Limestone and Arthur Creek Formation

How much of the apatite within the Thorntonia Limestone and Arthur Creek Formation must we account for with P delivery shuttles? Phosphorus speciation provides a (semi)quantitative measure of the partitioning of phosphorus within a sedimentary succession. The majority of P extracted from NTGS 99/1 is operationally classified as fluorapatite of detrital igneous and/or metamorphic origin (P_{xl}; Ruttenberg, 1992) and constitutes a median (1^{st}, 3^{rd} quartile) of 91.5% (77.5, 94.4) of P_T. However, we have three reasons to question this genetic interpretation. First, as described above, petrographic observations reveal that apatite within the Thorntonia Limestone occurs

predominantly as the internal molds of small shelly fossils (Fig. 3a) or, occasionally, as cement within bioclastic grainstone (Fig 3b), both indications of an authigenic origin. Given the thermal history of the Georgina Basin, which reached temperatures necessary to develop Type II kerogen (Dunster et al., 2007), burial diagenesis should have increased the crystallinity of authigenic phosphate minerals (Shemesh, 1990). It is thus not surprising that authigenic apatite formed within marine sediment during the Cambrian is now operationally classified as crystalline igneous and metamorphic apatite (*sensu* Föllmi et al., 2005). Second, within mud-supported, suspension-deposited carbonate, apatite occurs as coarse-silt- to medium-sand-size grains. Given that we observe no comparable size detrital siliciclastic grains, we suggest these grains are eroded, transported and winnowed authigenic grains. Third, if the P_{xl} phase comprised fluorapatite sourced to the basin along with a detrital siliciclastic influx, we would predict that it should correlate with the siliciclastic-associated heavy element Zr/Al ratio. We observe no correlation between P_{xl} and Zr/Al (Fig. 5f). Thus, consistent with petrographic observations, we conclude that the P_{xl} pool largely represents authigenic apatite and, therefore, we must account for this phase with a delivery shuttle of P to the sediment column.

Bioclastic apatite as a source of phosphorus for authigenic apatite precipitation?

Lingulid brachiopods comprise a fraction of the bioclasts identified in samples analyzed petrographically for carbonate sedimentology and apatite distribution. The presence of these phosphatic bioclasts raises two issues. First, samples that contain apatite bioclasts will have a wt.% P_T that overestimates the quantity of authigenic apatite. Determining the actual wt.% of P within authigenic apatite for these samples would require subtracting the

wt.% of bioclastic P from the bulk wt.% P_T determined by phosphorus speciation geochemistry. One method for determining the wt.% of P within primary phosphatic bioclasts would be to use quantitative point-count data to determine the volume of bioclasts, then to multiply this volume by the density of dahllite to determine the mass (wt.%) of P. Given that the percent of primary phosphatic bioclasts visually (qualitatively) rarely exceeds the percent of phosphatic steinkerns and sand-sized authigenic grains (see discussion above), we move forward without quantitative estimates of the wt.% of bioclastic P under the caveat that, for lingulid brachiopod-bearing bioclastic lithologies, P_T overestimates authigenic apatite within a sample.

Second, the observation of bioclasts of primary phosphatic shells raises the possibility that *in situ* dissolution of these bioclasts may have contributed to high pore-water phosphate concentration and facilitated subsequent authigenic precipitation. However, petrographic observations show that inarticulate brachiopod and other phosphatic skeletons are not unusually abundant in phosphate-rich Thorntonia horizons, and conversely that authigenic phosphate is not unusually abundant in those samples with the highest abundances of phopshatic skeletons. Nor do these remains show marked evidence of dissolution. Thus, the sedimentation of phosphatic skeletal material does not seem capable of sourcing the phosphate now found in Thorntonia rocks. Further, *in situ* dissolution of phosphatic bioclasts would necessitate pore fluids that promoted the early dissolution of apatite shells without concurrent dissolution of the calcium carbonate shells and sediment molded and/or replaced by the precipitation of authigenic calcium phosphate minerals. For these reasons, we do not invoke phosphatic skeleton-derived P as a significant source for authigenic apatite precipitation. Nevertheless, if phosphatic

skeleton dissolution were to have sourced P for authigenic apatite, then the required quantity of organic and iron-bound P (discussed below) would lessen proportionately.

Organic-bound phosphorus as a source of phosphorus for authigenic apatite precipitation?

Particulate organic carbon represents the main delivery shuttle of phosphorus to the sediment column in the modern ocean (e.g., Delaney, 1998; Benitez-Nelson, 2000), and so we ask whether organic carbon could have sourced the observed amount of P within beds of the Thorntonia Limestone and the Arthur Creek Formation. Perhaps the simplest model for organic-bound P delivery is to assume that organic matter arrived at the sea floor with a Redfield C_{org}:P_{org} molar ratio of ~106:1 (Redfield, 1958). However, C_{org}:P_{org} of organic matter within marine sediment and, therefore, sedimentary rocks, is commonly much higher than the Redfield ratio as a result of the preferential remineralization of P-rich organic compounds within the water-column (Clark et al., 1998) or within the sediment column (Ingall et al., 1993, Ingall and Jahnke, 1997; Van Cappellen and Ingall, 1996; Jilbert et al., 2011). C_{org}:P_{org} molar ratios within the Thorntonia Limestone range from 79:1 up to 17,000:1 [median (1^{st}, 3^{rd} quartile) = 1,389:1 (521:1, 3619:1)]. Likewise, C_{org}:P_{org} molar ratios within the Arthur Creek Formation range from 43:1 up to 11,770:1 [median (1^{st}, 3^{rd} quartile) = 903:1 (360:1, 3,372:1)]. Thus, C_{org}:P_{org} molar ratios within these lithologies deviate substantially from the Redfield ratio and, at face value, suggest extensive preferential P_{org} loss during organic matter respiration.

When organic respiration occurs within the sediment column, liberated P_{org} may 'sink-switch' and precipitate as authigenic phosphate minerals (Ruttenberg and Berner,

516 1993), as is likely the case for the development of phosphatic strata within the Thorntonia
517 Limestone. With respect to phosphorus speciation terminology, ‘sink-switching’ would
518 transfer P from the P_{org} phase to either the authigenic P_{xl} or the $P_{auth+carb}$ phase. In that
519 regard, C_{org}:P_T should provide a better estimate of the retention of organic-bound P to the
520 sedimentary environments of the Thorntonia Limestone and Arthur Creek Formation
521 (Ingall et al., 1993; Ruttenberg and Berner, 1993; Anderson et al., 2001; Algeo and Ingall,
522 2007). C_{org}:P_T ranges from 0.1–16:1 within the Thorntonia Limestone with a median (1^{st},
523 3^{rd} quartile) value of 2.5:1 (1.2:1, 4.8:1). For the non-phosphatic Arthur Creek Formation,
524 C_{org}:P_T ranges from 5–157:1 with a median (1^{st}, 3^{rd} quartile) value of 17.4:1 (7.6:1,
525 44.5:1). Thus, with the exception of four samples, C_{org}:P_T molar ratios for both the
526 Thorntonia Limestone and the Arthur Creek Formation fall well below the canonical
527 Redfield ratio (Fig. 5d). From this perspective, both the Thorntonia Limestone and the
528 Arthur Creek Formation retain more P than would be expected based on organic matter
529 delivery with a molar C_{org}:P_{org} ratio equal to or greater than the Redfield ratio.
530 Preferential C_{org} remineralization or hydrocarbon migration relative to P retention
531 may have resulted in a molar C:P_T lower than the Redfield ratio. The required > 90% loss
532 of C_{org} (see below) appears to be common in relatively organic-lean sediment deposited
533 on oxic Cenozoic seafloors (Anderson et al., 2001); however, given the organic carbon
534 content of Thorntonia samples, and accepting sedimentological and geochemical
535 arguments for anoxic deposition of the Thorntonia Limestone (see below), such loss
536 would have required massive remineralization under anoxic pore water conditions.
537 $\delta^{13}C_{carb}$ values do not show the distinctly light values that might be expected in this
538 circumstance (Schrag et al., 2013). Assuming that all phosphorus was delivered via

539 organic matter with a Redfield ratio and was subsequently retained within the sediment
540 column, the discrepancy between the Redfield ratio and the measured $C:P_T$ provides a
541 minimum estimate of C_{org} loss (estimated quantitatively in a later section).
542 Organic carbon loss may also occur during low-grade metamorphism (Raiswell
543 and Berner, 1987). Since the lithology of the Thorntonia Limestone precludes a confident
544 application of the suggested metrics to account for this loss (Raiswell and Berner, 1987),
545 we cannot evaluate how much this process may have contributed to the discrepancy
546 between measured $C_{org}:P_T$ values and the Redfield ratio. However, we can explore
547 whether an additional phosphorus delivery shuttle augmented organic-bound P delivery
548 to the sea floor during deposition of the Thorntonia Limestone and Arthur Creek
549 Formation. We discuss this possibility in a later section.
550 Notably, phosphatic strata of the middle Thorntonia Limestone have the highest
551 measured wt. % TOC and the lightest $\delta^{13}C_{org}$ values preserved within this sedimentary
552 succession (Fig. 4c). A similar relationship has been document in Proterozoic basins and
553 attributed to differential recycling of organic matter in benthic mats (e.g., Bartley et al.,
554 1998; Guo et al., 2013). Within the Thorntonia Limestone, this relationship may result
555 from a difference in the primary isotopic composition of organic matter sourcing
556 phosphatic strata, from variable *in situ* remineralization of the sedimentary organic
557 carbon reservoir, or from some combination of these two processes. We do not have an
558 independent line of evidence (e.g., compound specific biomarkers) to distinguish between
559 these possibilities. Instead, we note that acceptance of either of these hypotheses to
560 explain the observed correlation between P content and $\delta^{13}C_{org}$ values makes a prediction
561 for the mechanism of P delivery. For the case of an isotopically distinct organic carbon

source to the middle Thorntonia Limestone, the C:P ratio of this source must have been much lower than the canonical Redfield ratio of 106C:1P. For the case of limited C_{org} remineralization within phosphatic strata, an alternative P delivery shuttle to the sediment column must have augmented organic-bound P delivery.

Iron-bound phosphorus as a source of phosphorus for authigenic apatite precipitation?

If our estimates of organic-bound P delivery fail to account for the phosphate necessary for the observed Thorntonia apatite content, what alternative source could supply this P? A growing body of literature calls upon P adsorbed to the surface or co-precipitated with metal oxides, particularly iron (oxyhydr)oxide particles, as an important shuttle of phosphorus to the sea floor (Berner, 1973; Shaffer, 1986; Feely et al., 1991; Feely et al., 1998; Poulton and Canfield, 2006). Additionally, under anoxic conditions, Fe(II)-phosphates (e.g., vivianite, strengite) may play a more important role for marine P cycling than previously considered (e.g., März et al., 2008; Dellwig et al., 2010; Jilbert and Slomp, 2013). Thus, the release of adsorbed/co-precipitated Fe-bound P to sediment pore waters has previously been invoked as a necessary and significant source of P for sedimentary apatite nucleation (Krom and Berner, 1981; Schuffert et al., 1994, 1998; Slomp et al., 1996; Shen et al., 2000; März et al., 2008; Jilbert and Slomp, 2013).

Could the Fe-P shuttle have augmented organic-bound P delivery to Thorntonia and Arthur Creek sediments? In the modern, oxygenated ocean, iron mobility is generally limited to particulate fluxes of insoluble Fe^{3+} phases (Martin and Meybeck, 1979; Poulton and Raiswell, 2002). Under these conditions, we might predict Fe-bound P

585 delivery to these environments to be proportional to the (predominantly siliciclastic)
586 particulate Fe(III) flux. In contrast, under anoxic conditions the reductive dissolution of
587 iron (oxyhydr)oxides by dissimilatory iron reduction or by dissolved sulfide during early
588 diagenesis generates soluble Fe^{2+} that is subsequently redistributed to anoxic slope and
589 basinal environments (Canfield et al., 1996; Severmann et al., 2008; 2010; see review in
590 Lyons and Severmann, 2006). This so-called 'intrabasin iron shuttle' provides a
591 mechanism for decoupling iron delivery to the seafloor from siliciclastic sources and,
592 therefore, we hypothesize that it allows for the delivery of P adsorbed to detrital Fe(III)
593 minerals, Fe(II)-phosphate minerals (e.g., März et al., 2008; Dellwig et al., 2010; Jilbert
594 and Slomp, 2013) and P adsorbed to/co-precipitated with Fe(III)-minerals formed from
595 the oxidation of ferrous iron in the water column (*cf.*, Mayer and Jarrell, 2000). In this
596 regard, under either an oxic or an anoxic Cambrian water-column, Thorntonia and Arthur
597 Creek sediments could have received substantial Fe-bound P; however, we note that the P
598 contribution from the Fe-bound P shuttle would have been larger if these sediments
599 accumulated under an anoxic water column.

600 The redox state of the southern Georgina Basin water column during deposition of
601 these middle Cambrian strata can be assessed using data on the speciation and enrichment
602 of sedimentary iron minerals. This geochemical method is most commonly applied to
603 fine-grain siliciclastic lithologies, where the ratios of various mineralogical phases are
604 interpreted to reflect specific and calibrated environmental redox conditions (Canfield et
605 al., 1992; Raiswell and Canfield, 1998; Raiswell et al., 2001; Poulton and Raiswell,
606 2002). On the basis of empirical evidence, Fe_{HR}/Fe_T above 0.38 within fine-grain
607 siliciclastic lithologies indicates sediment accumulation under an anoxic water-column

(Raiswell and Canfield, 1998; Raiswell et al., 2001; Poulton and Raiswell, 2002), while Fe_{HR}/Fe_T below a value of ~0.22 is suggestive of oxic conditions (Poulton and Raiswell, 2002; Poulton and Canfield, 2011); additionally, in the case of anoxia, Fe_{py}/Fe_{HR} differentiates ferruginous (<0.7-0.8) from euxinic (>0.8) conditions (Anderson and Raiswell, 2004; Poulton et al., 2004; März et al., 2008; Poulton and Canfield, 2011).

The Arthur Creek Formation includes a siliciclastic facies (the 'hot shale') that is ideal for iron-based redox proxies (Poulton and Canfield, 2005). Fe_T within the Arthur Creek 'hot shale' ranges up to ~2.7 wt.% (Fig. 6a) and almost all measured highly reactive iron resides in reduced iron minerals (Fig. 6b,c). Fe_{HR}/Fe_T and Fe_{PY}/Fe_{HR} indicate an anoxic, ferruginous redox environment during deposition of the 'hot shale' (Fig. 6a,b). In contrast, strata of the interlaminated siliciclastic shale/siltstone and carbonate calcimudstone facies of the Arthur Creek Formation (directly overlying the 'hot shale') contain a lower siliciclastic component, and this requires special attention in interpreting a paleo-redox environment. We note that each iron-speciation sample integrates 3 cm of stratigraphy; therefore, for this lithofacies, our sample preparation method homogenized multiple laminae of pure siliciclastic shale/siltstone and pure carbonate mudstone. Yet, despite the diluting carbonate component, Fe_{HR} is partitioned within this lithofacies in the same proportionality as the 'hot shale' (Fig. 6b,c). In this regard, iron speciation data for this lithofacies of the Arthur Creek Formation are consistent with the anoxic, ferruginous redox environment inferred for the underlying 'hot shale'.

Strata of the Thorntonia Limestone are composed almost entirely of carbonate, and for this reason we do not to interpret these iron speciation data within the canonical,

siliciclastic-derived redox framework. Instead, we emphasize that the black, organic-rich carbonate strata of the middle/upper Thorntonia Limestone (Fig. 2c), biomarker and organic geochemistry of the Thorntonia and Arthur Creek petroleum systems (Boreham and Ambrose, 2005), and trace element data (Supplementary Information) are qualitatively consistent with iron speciation metrics for the Arthur Creek Formation 'hot shale' (Fig. 6) for an anoxic depositional environment during accumulation of the phosphatic middle/upper Thorntonia Limestone. Thus, we conclude that the Fe-oxide bound P shuttle likely augmented organic-bound P delivery to the Thorntonia and Arthur Creek sediment column. Further, if one accepts the sedimentological and geochemical evidence for sediment accumulation under an anoxic, ferruginous water column, this then allows for the possibility that Fe(II)-phosphates provided a second, potentially significant source of P to Thorntonia sediments.

Nevertheless, the limited contribution of Fe_{ox} to Fe_{HR} in both the Thorntonia and Arthur Creek (Fig. 5c), the low P_{Fe} values (Fig. 5b), and the present decoupling of P within the Thorntonia from Fe_{HR} phases (Fig. 5g) all suggest that any P delivered to Thorntonia sediments via the Fe-P shuttle must have been subsequently decoupled from iron particles within the sediment column. One way to explain this decoupling is through the reductive dissolution of Fe oxides in anoxic pore-waters. This suggestion is consistent with petrological observations that require wholesale remobilization of P before precipitation within shell interiors (Fig. 3a,b). Thus, the present distribution of P in the Thorntonia Limestone, spatially decoupled from either iron or organic carbon sources, confounds easy attribution to primary source vectors. In the following section we

integrate C, Fe, and P geochemical data to explore the relative contribution from organic-bound and iron-bound P delivery sources.

Assessing the relative importance of organic-bound versus iron-bound phosphorus to authigenic apatite precipitation

To begin, we estimate whether organic matter degradation alone could provide sufficient phosphorus for the observed apatite content in the Thorntonia Limestone. We then quantify how much of this estimated organic carbon must have been lost through remineralization to reconcile the observed wt.% TOC within these strata. To do so, we use a Redfield stoichiometry (Redfield, 1958) to relate the measured sedimentary weight percent phosphorus to the associated flux of organic carbon necessary for this phosphorus delivery. Redfield stoichiometry varies in space and time due to, for instance, taxonomic variability in biomolecular and cellular composition and nutrient availability regulating biosynthetic allocation (e.g., Geider and LaRoche, 2002). Moreover, water-column heterotrophy increases the C:P ratio of particulate organic carbon delivered to the sediment-water interface (Clark et al., 1998). To be conservative, we assume no water-column remineralization and adopt the canonical Redfield ratio (106C:1P) in the calculations below. We also adopt the combined organic-bound and authigenic phosphorus phases determined from the phosphorus speciation extraction as an estimate of the original flux of phosphorus delivered to the sediment via organic matter. This calculation provides a conservative estimate because we neglect iron-adsorbed and carbonate-bound P as potential sources for authigenic apatite (as these can represent

675 primary sources of phosphorus to the sediment column), and we assume no diffusive loss
676 of phosphate from pore-water contemporaneous with sedimentary apatite authigenesis.
677 Following the above arguments, our estimate for the weight percent organic
678 carbon delivered to the sediment column ($\hat{C}^*_{org}$) that can account for the measured
679 phosphorus content is given by:

680 $$\hat{C}^*_{org} = \left(P_{xl} + P_{org}\right) \times R \times \left(\frac{\alpha_c}{\alpha_p}\right) \quad (1)$$

681 where R is the adopted Redfield ratio and α_C and α_P represent the molar weights of
682 carbon and phosphorus, respectively (Slomp et al., 2004). We estimate the percentage of
683 organic carbon remineralization necessary to reconcile the difference between the
684 delivery estimate, $\hat{C}^*_{org}$, and the measured wt.% total organic carbon (C_{org}) within
685 Thorntonia and Arthur Creek rocks (Slomp et al., 2004) as:

686 $$\%\, loss\ of\ \hat{C}^*_{org} = \left(\frac{\hat{C}^*_{org} - C_{org}}{\hat{C}^*_{org}}\right) \times 100\ . \quad (2)$$

687 This value represents an estimate of organic carbon remineralization in the time between
688 delivery to the sediment-water interface and lithification. Applying these equations to
689 samples within the phosphorus-enriched middle and upper Thorntonia yields a median
690 $\hat{C}^*_{org}$ of 18.6 wt.% and a median loss of 97.8% of this estimated delivery flux (Fig. 7). For
691 comparison, applying these equations to samples from the Arthur Creek indicates a
692 median organic carbon loss estimate of 74.0% from a median organic carbon delivery
693 estimate, $\hat{C}^*_{org}$, of only 1.1 wt.% (Fig. 7). If, instead, we consider more typical ratios of
694 C_{org}:P_{org} delivered to the sediment column, that is, C:P >> 106:1 (Ingall et al., 1993; Van
695 Cappellen and Ingall, 1996; Clark et al., 1998; Algeo and Ingall, 2007), then the required

696 C_{org} delivery ($\hat{C}^{*}_{org}$) and the estimated % $\hat{C}^{*}_{org}$ loss increase proportionally. Likewise, any
697 diffusive/advective loss of phosphate from the sediment column prior to lithification
698 (Ingall et al., 1993; Slomp et al. 2002; 2004) would increase the requisite $\hat{C}^{*}_{org}$ and, thus,
699 the inferred % $\hat{C}^{*}_{org}$ loss.

700 If organic carbon represented the sole delivery source of phosphorus to the
701 sediment column, what would have been the oxidant demand for the organic carbon
702 remineralization estimated above? Dissimilatory microbial metabolisms couple the
703 remineralization of sedimentary organic carbon to the reduction of an oxidant (primarily
704 O_2, NO_3^-, SO_4^{2-}, and Fe^{3+}; Konhauser, 2007). Thus, a portion of the estimated organic
705 carbon loss can be accounted for in the early diagenetic minerals pyrite and siderite,
706 which form from microbial dissimilatory sulfate and ferric iron respiration, respectively.
707 In the following calculations, we assume the stoichiometry of Fe-(oxyhydr)oxide
708 reduction, where one mole of organic carbon is remineralized per four moles of siderite
709 produced:

710 $$CH_2O + 8H^+ + 4Fe(OH)_3 \Rightarrow 4Fe^{2+}_{(aq)} + CO_2 + 11H_2O \quad (3)$$

711 $$4Fe^{2+}_{(aq)} + 4CO_2 + 4H_2O \Rightarrow 4FeCO_3 + 8H^+, \quad (4)$$

712 and sulfate reduction, where four moles of organic carbon are remineralized per mole of
713 pyrite produced:

714 $$4CH_2O + 2SO_4^{2-} \Rightarrow 2H_2S + 4HCO_3^- \quad (5)$$

715 $$Fe^{2+}_{(aq)} + 2H_2S \Rightarrow FeS_2 + 4H^+ . \quad (6)$$

716 We note that if Fe^{2+} for pyrite formation were also reduced locally it would require
717 additional C_{org} consumption, akin to Eqn. (3).

718 To correct for the presence of siderite within samples, we relate the measured
719 molar quantity of siderite to the Fe^{3+} respiration stoichiometries of Eqns. 3 and 4 to
720 estimate the necessary weight percent of organic carbon consumed to produce this
721 siderite ($C_{siderite}$):

722 $$C_{siderite} = \left(\frac{\left[measured\ siderite(mol) \times \left(\frac{1\ mol\ C_{org}}{4\ mol\ siderite} \right) \right] \times \gamma}{sample\ weight\ (g)} \right) \times 100 \quad (7)$$

723 where γ converts measured values in moles to wt.%. Likewise, to correct for the presence
724 of pyrite, we relate the measured molar quantity of pyrite within each sample to the
725 stoichiometry of SO_4^{2-} respiration (Eqns. 5 and 6) in order to estimate the weight percent
726 of organic carbon remineralized to produce this pyrite (C_{pyrite}):

727 $$C_{pyrite} = \left(\frac{\left[measured\ pyrite\ (mol) \times \left(\frac{4\ mol\ C_{org}}{1\ mol\ pyrite} \right) \right] \times \gamma}{sample\ weight\ (g)} \right) \times 100 \quad . \quad (8)$$

728 Equation (8) does not account for any C_{org} consumed to reduce iron for pyrite (e.g., Eqn.
729 3). In this regard, Eqns. 8 and 9 conservatively underestimate the weight percent of
730 organic carbon remineralized to form pyrite for the case that iron was reduced locally,
731 rather than sourced as Fe^{2+}.
732 With these estimates, we augment Eqn. (2) as:

733 $$\left(\frac{\hat{C}^*_{org} - \left(C_{org} + C_{pyrite} + C_{siderite} \right)}{\hat{C}^*_{org}} \right) \times 100 \quad . \quad (9)$$

734 This exercise yields a corrected median % $\hat{C}^*_{org}$ loss for the middle and upper Thorntonia
735 members of 96.2%, not significantly different than the estimate from Eqn. 2 (Fig. 7). In
736 contrast, and with the exception of phosphorus-enriched samples in the uppermost
737 measured meters, the corrected median loss for the Arthur Creek indicates that there is an

738 excess wt.% of organic carbon to account for the observed wt.% phosphorus (Fig. 7).
739 However, the observed quantity of siderite within Thorntonia and Arthur Creek samples
740 may represent a late diagenetic addition to the sediment column and, thus, may not have
741 formed through local iron respiration consuming C_{org}. If this were the case, the % C_{org}
742 loss would be less than the value estimated by Eqn. (9), and closer to the value
743 determined by Eqn. (2).

744 With sulfate and ferric iron accounted for, the only quantitatively important
745 remaining oxidant is molecular oxygen (Konhauser, 2007). In this regard, and if the
746 above assumptions hold, the implication is that the majority of the hypothesized organic
747 carbon loss was through respiration using molecular oxygen. We define a ratio of the
748 estimate of organic matter consumed through anoxic respiration (that is, with Fe^{3+} and
749 SO_4^{2-}: $C_{siderite}$ and C_{pyrite}, respectively) to the estimate of C_{org} loss not accounted for by
750 this estimated anoxic remineralization. We calculate the ratio of anoxic to oxic
751 respiration as:

752 $$\frac{anoxic}{oxic}\ respiration = \frac{C_{pyrite}+C_{siderite}}{\hat{C}^{*}_{org} - (C_{org}+ C_{pyrite}+C_{siderite})}\,. \qquad (10)$$

753 In solving Eqn. (10), we obtain a median (1st, 3rd quartile) value of 0.02 (0.1, 0.4) for the
754 middle and upper Thorntonia members. This is to say that a median 2% of the estimated
755 organic carbon delivery required to source the observed phosphorus content was
756 remineralized through anoxic pathways—98% must have been remineralized with
757 molecular oxygen to explain the absence of this organic carbon from measured samples.
758 If, however, one assumes a diffusive loss of either sulfide or ferrous iron from the
759 sediment column (i.e., the numerator underestimates the organic carbon consumed by
760 anoxic remineralization), the estimated percent of anoxic remineralization becomes a

761 minimum. If such diffusive loss occurred, then the proportion of C_{org} remineralized
762 through oxic respiration would be less than 98% and approach 0% as the sedimentary
763 production of sulfide and/or Fe^{2+} through microbial dissimilatory redox reactions
764 quantitatively consumed $\hat{C}^{*}_{org}$. While we cannot determine the diffusive flux of
765 reductants from Thorntonia or Arthur Creek sediments based on preserved geochemical
766 signals, we note that such a diffusive loss would be possible if the redox boundary
767 resided within the water column.
768 The calculated weight percent organic carbon required to deliver the observed
769 phosphorus is notable; the median value, 18.6 wt.%, exceeds organic carbon export to the
770 sea floor in most modern marine environments (Hedges and Keil, 1995). While such low
771 organic carbon preservation efficiencies (or, as we describe, high % $\hat{C}^{*}_{org}$ loss estimates)
772 commonly occur within modern marine environments, they typify depositional
773 environments with low sediment accumulation rates (< ~0.02 cm/yr) or oxygenated shelf
774 settings (> 20 μM bottom-water O_2; Canfield, 1994; Hedges and Keil, 1995). While we
775 cannot provide unequivocal evidence that substantial aerobic carbon respiration did not
776 consume most of the C_{org} originally delivered to the Thorntonia sediment column, we
777 find it difficult to reconcile how such substantial aerobic respiration could have
778 proceeded without concurrently driving the sediment column anoxic, providing a
779 negative feedback on the efficiency of organic carbon respiration. Moreover, we note that
780 the oxidant demand to remineralize this magnitude of organic carbon is difficult to
781 reconcile with Cambrian oxygen levels, perhaps 15 – 50% present atmospheric
782 concentrations (Dahl et al., 2010; Bergman et al., 2004; for alternative views, see Berner,
783 2006; Garrels and Lerman, 1984). Nevertheless, it remains a possibility that episodes of

784 intense aerobic respiration—and efficient capture of released P within authigenic
785 phases—account for Thorntonia Limestone phosphatic carbonate precipitation (although
786 see Föllmi et al. (2005) for discussion of a Miocene phosphogenic episode in which P
787 sourced from aerobic respiration was ruled out). If, however, one accepts the conclusion
788 that organic burial alone does not provide an adequate source of phosphorus to the
789 sediment column, then an additional source of P must have been present during
790 Thorntonia deposition.

791 Phosphorus adsorbed onto and/or co-precipitated with metal oxide particles
792 provides a second potential source of P to the sediment column whose importance
793 depends, in part, on the magnitude of the flux of metal oxides to the sediment column
794 (Shaffer, 1986; Feely et al., 1990; Feely et al., 1998; Poulton and Canfield, 2006).
795 Accordingly, we estimate phosphorus delivery under the assumption of an appreciable
796 iron-bound P flux, for simplicity based entirely on P adsorbed to iron (oxyhydr)oxides.
797 This assumption is consistent with the order-of-magnitude calculations presented above;
798 nonetheless, we acknowledge that other metal oxides, particularly manganese, play an
799 important role in the cycling of phosphorus (e.g., Dellwig et al., 2010).

800 Ideally, iron-speciation measurements could provide the basis for a quantitative
801 estimate of Fe-bound P delivered to the sediment column. But before we can perform
802 such a calculation, we ask whether the Fe_{ox}, Fe_{mag}, Fe_{carb}, and Fe_{py} pools as determined by
803 iron speciation in carbonate-rich strata of the Thorntonia Limestone and Arthur Creek
804 Formation reflect primary depositional reservoirs, or if post-depositional diagenesis could
805 have converted iron into, out of, or between these phases of the highly reactive iron pool?
806 Specifically, if these lithologies experienced closed system (with respect to mass)

807 diagenetic remobilization of Fe, then it is likely that appreciable amounts of Fe were
808 transferred between highly reactive iron phases (e.g., the formation of Fe_{carb} and Fe_{py}
809 through the reduction of an Fe_{ox} precursor phase). In this regard, the value for Fe_{HR} would
810 still accurately represent the primary iron pool—and could thus be used in calculations of
811 Fe-bound P delivery—however calculations involving any individual Fe_{HR} phase (e.g.,
812 Fe_{ox}, Fe_{carb}) would not provide robust estimates of Fe-bound P. Alternatively, if these
813 lithologies underwent open system diagenesis, the resulting addition or loss of Fe from
814 the Fe_{HR} pool (from any and/or all constituent phases) would render *any* calculation based
815 on the iron speciation data suspect. While we cannot eliminate the possibility of Fe
816 addition during open system diagenesis, we note that Fe-speciation data for the
817 Thorntonia Limestone and Arthur Creek Formation are consistent with other redox
818 proxies (see above) favoring the view that the highly reactive iron species to these rocks
819 record a substantial depositional flux.
820 In the following discussion we provide a methodology to address the potential
821 contribution of the Fe-P shuttle to Thorntonia and Arthur Creek sediments under the
822 assumption of limited or closed system iron diagenesis. To this end, we employ iron
823 speciation data from these lithologies for illustrative calculations. These calculations
824 provide a consistency argument given that organic-bound P was likely insufficient to
825 account for the measured P content. Throughout this discussion, we introduce and
826 emphasize the caveats inherent to the use of a diagenetically mobile element in these
827 calculations.
828 The molar ratio of the co-precipitation of phosphorus onto iron (oxyhydr)oxide
829 particles conforms to a distribution coefficient (K_D) model that scales linearly to the

ambient seawater phosphate concentration ([P_{sw}]) (Feely et al., 1991; 1998; Konhauser et al., 2007):

$$\left(\frac{P}{Fe}\right)_{molar} = K_D \times \left[P_{SW}\right]. \quad (11)$$

Thus, to estimate the delivery of iron-bound phosphorus, $\hat{P}^{*}_{Fe}$, we multiply an estimate of iron oxide delivery ($\hat{F}e^{*}_{ox}$) by the adsorption coefficient of phosphorus to iron oxides (K_D) for a given estimate of seawater phosphate concentration ([P_{sw}]):

$$\hat{P}^{*}_{Fe} = \gamma \hat{F}e^{*}_{ox} \times K_D \times \left[P_{SW}\right] \quad (12)$$

where γ converts measured values (in wt.%) to moles as required in the definition of the adsorption coefficient. Within anoxic pore-waters, a fraction of the iron oxides delivered to the sediment column will be reduced by dissimilatory iron reduction and converted to ferrous iron, and these ions will either precipitate as pyrite or iron carbonate, or advect/diffuse to the overlying water column. Accordingly, a full accounting of $\hat{F}e^{*}_{ox}$ would include all of these conservation and loss terms. The estimate would become a lower bound on $\hat{P}^{*}_{Fe}$ if we ignored the ferrous iron loss flux, which in any event is unconstrained, and included only the measured iron oxide (Fe_{ox}), pyrite (Fe_{py}) and iron-carbonate phases (Fe_{carb}). We note, however, that at least some of the measured Fe (most obviously the Fe_{carb} phase) may have originated from diagenetic remobilization of iron to these carbonates. (For the lower Thorntonia Limestone, Fe_{carb} comprises a median (1st, 3rd quartile) of 76.8 % (71.3, 81.8) of the total iron pool; in contrast, for the phosphatic middle/upper Thorntonia and for the Arthur Creek Formation, Fe_{carb} accounts for only

28.7 % (22.3, 33,2) and 20 % (15.15, 23.5) of Fe_T, respectively.) In this regard, this calculation may overestimate $\hat{P}^*_{Fe}$.

Magnetite may form through the reductive dissolution of mixed ferrous–ferric oxide phases (e.g., Zegeye et al., 2012), and, as such, could be considered in the summation of primary iron oxide minerals ($\hat{F}e^*_{ox}$); however, magnetite may also form during prograde metamorphism, in which case inclusion of this phase would over-estimate the primary ferric iron flux to the sediment column. We include Fe_{mag} within our calculation because the authigenic pathway likely exceeds weathering and metamorphic overprints for this depositional environment. (Regardless, within NTGS 99/1 magnetite represents a negligible component of Fe_T, therefore this assumption does not alter the illustrative estimate for $\hat{P}^*_{Fe}$.) Therefore, we rewrite Eqn (12) in the approximate form:

$$\hat{P}^*_{Fe} = \gamma\left(Fe_{ox} + Fe_{py} + Fe_{carb} + Fe_{mag}\right)\times K_D \times [P_{SW}]\,. \quad (13)$$

A host of seawater ions—notably silica, trace metals and rare earth elements—compete with phosphorus for adsorption sites on the surface of iron oxide particles (e.g., Berner, 1973; Trocine and Trefry, 1988; Olivarez and Owen, 1989; Trefry and Metz, 1989; Feely et al., 1991; Feely et al., 1998; German et al., 1990; Konhauser et al., 2007). Thus, the choice of K_D depends on the assumption of the seawater composition of Cambrian oceans. As these element concentrations are broadly unknown for the Paleozoic Era, we focus here only on the role of the major seawater constituent dissolved silica in competition for iron-surface anion sites. Following Siever's (1992) inference of cristobalite saturation for early Phanerozoic seawater ($[Si_{SW}]$ = 0.67 mM), Konhauser et al. (2007) determined experimentally a K_D = 0.0108 for ferrihydrite at this silica saturation state. Notably, the linear range of the K_D model depends on the phosphorus

concentration of ambient seawater. At cristobalite saturation, the linearity of the K_D model saturates above ~5 μM [P_{sw}]. This is to say that the co-precipitation and delivery of phosphorus bound to iron oxides remains constant at and above this ambient seawater phosphate concentration.

Hence, we adopt [P_{sw}] = 5 μM to calculate a maximum estimate for $\hat{P}^{*}_{Fe}$ at the adopted [Si_{SW}]. We emphasize that the chosen value of 5 μM is a simplistic assumption and that water column phosphorus concentrations are affected by variable environmental factors that are difficult to generalize, even under well-constrained modern conditions. Nevertheless, this adopted phosphate concentration is consistent with modern anoxic environments, including the Black Sea and Cariaco Basin (Shaffer, 1986; Scranton et al., 2006). For example, in the Black Sea, higher phosphate concentrations in the ferruginous chemocline than in the underlying sulfidic waters result from the dissolution of settling Fe-oxides and the release of adsorbed phosphate (Brewer and Murray, 1973). Similar processes are suggested to explain the phosphate concentrations (up to 9 μM dissolved P) in the ferruginous Lake Matano (Crowe et al., 2008) where the release of Fe(III)-bound P at the chemocline is balanced by the precipitation of Fe(II)-phosphates below the chemocline.

Applying Eqn. (13) to samples from the middle and upper Thorntonia members yields a median estimate for iron-bound P of 0.1 wt.% as compared to a median estimate of 0.2 wt.% for the Arthur Creek (Fig. 7). In this formulation, phosphorus delivery by iron oxides is proportional to the highly reactive iron phases (Fe_{HR}) determined from iron speciation geochemistry. While Fe_{HR}/Fe_T decreases between the P-enriched middle / upper Thorntonia members and the Arthur Creek, the observed increase in Fe_T within the

Arthur Creek compensates such that the molar estimate of $\hat{Fe}^{*}_{ox}$, and, thus, $\hat{P}^{*}_{Fe}$ remains roughly constant between the two formations. As such, and if the above assumptions hold, this implies that the relative contribution of the Fe-P shuttle to the observed weight percent sedimentary P was much greater during deposition of the Arthur Creek Formation because of the lower wt.% P_T measured throughout this formation. Indeed, the median estimate of $\hat{P}^{*}_{Fe}$ = 0.2 wt.% for the Arthur Creek greatly exceeds the median measured P_T (0.03 wt.%; Fig. 7). In contrast, the median estimate of $\hat{P}^{*}_{Fe}$ = 0.1 wt.% for the middle and upper Thorntonia members provides only ~10% of the median measured P_T (0.98 wt.%; Fig. 7), and proportionally less for samples with the highest measured P_T approaching 4 wt.%. Likewise, any diffusive loss of P from the sediment column prior to lithification would increase the requisite $\hat{P}^{*}_{Fe}$ and, in the case of the Thorntonia, increase the deficiency between the observed P_T and P hypothesized to have been delivered associated with Fe_{ox} ($\hat{P}^{*}_{Fe}$).

The formulation of our equations may significantly overestimate Fe-bound P delivery for two reasons. First, our calculations adopt a K_D value based on an estimate of contemporaneous seawater silica concentrations. Second, our calculations adopt a seawater phosphate concentration that maximizes the potential for phosphorus delivery by the iron shuttle. If we presumed a higher seawater silica concentration (that is, decreased K_D), or if, for an assumed [Si_{SW}], we also assumed a lower [P_{SW}], then we would calculate a lower P delivery flux per unit Fe_{ox}. Thus, both of these changes would yield a lower estimate of $\hat{P}^{*}_{Fe}$ for a given iron flux to the sediment column.

Some iron minerals are more effective P delivery shuttles than others. The capacity for iron minerals to scavenge and deliver phosphorus to the sea floor depends on a number of factors, including the surface density of adsorption sites, which in part is related to mineral surface area. In this regard, amorphous to poorly crystalline phases will scavenge more phosphate than highly crystalline phases. (We note, however, that progressive crystallization may result in the subsequent desorption of P from adsorption sites. If this desorption occurs within the sediment column, outside the length-scales of advection/diffusion with the overlying water-column, Fe-bound P could provide a significant source of P to the sediment column.) Here we assumed ferrihydrite as the carrier phase (Konhauser et al., 2007), however, a range of other iron minerals form during anaerobic Fe^{2+} oxidation (e.g., Kappler and Newman, 2004; Zegeye et al., 2012). For instance, in the only detailed study of Fe mineralogy in a ferruginous water column (Lake Matano, Indonesia), Zegeye et al. (2012) found that ferrihydrite was quantitatively transformed to carbonated green rust ('fougerite') during settling through the water column, with more minor formation of magnetite. Unfortunately, no experimental data currently exist for P adsorption to green rust under the chemical conditions likely encountered in Cambrian oceans (e.g., Lake Matano has relatively low [Si]). However, adsorption of oxyanions to green rust tends to be far higher than for ferrihydrite (Randall et al., 2001), and thus such a finding highlights the need to consider multiple and varied carrier phases for the ancient Fe-P shuttle. An iron carrier phase with an adsorption coefficient (K_D) with respect to P greater than ferrihydrite could have delivered more P to Thorntonia sediments for a given iron flux to the sea floor.

939 Are there other scenarios in which the delivery of Fe-bound P could have been
940 greater than that inferred from the formulations of equations 11 through 13? To answer
941 this question it is necessary to address whether the measured Fe_{HR} is an accurate proxy
942 for the contribution of Fe_{ox} to the sediment column, or whether it could underestimate the
943 original Fe_{ox} flux ($\hat{Fe}^{*}_{ox}$), and, thus, $\hat{P}^{*}_{Fe}$ to the sediment column. Next, we explore
944 hypothetical redox scenarios in which Fe-bound P could contribute more substantially to
945 authigenic apatite. Without an independent line of evidence that the constituent phases of
946 the highly reactive iron pool represent the primary fluxes of iron to the sediment column,
947 we choose not to advocate for this possibility for the Thorntonia Limestone.
948 Nevertheless, with regard to the broader question of the mechanism for phosphatic
949 carbonate deposition, we find it informative to evaluate the circumstances in which the
950 Fe-bound delivery shuttle could contribute substantially to phosphogenesis and
951 phosphatic carbonate deposition.
952 One can envision a spectrum of scenarios for the relative magnitudes of Fe_{ox}
953 delivery to and Fe^{2+} loss from the sediment column. These scenarios fall within three
954 generalized categories: Fe_{ox} delivery (1) greater than, (2) nearly equal to, or (3) less than
955 Fe^{2+} diffusive/advective loss. In the following discussion we discount scenario (3)
956 because such an imbalance defines an unsustainable Fe cycle. To begin, we consider the
957 scenario that (1) Fe_{ox} delivery exceeds Fe^{2+} loss. This can result from two opposing redox
958 regimes. (1a) If the majority of Fe_{ox} delivered to the sediment column were stabilized
959 within oxygenated pore-water then this would preclude widespread iron reduction. In this
960 instance, only a small amount P would be liberated from the Fe_{ox} delivery shuttle, and
961 Fe_{ox} would dominate Fe_{HR}. (1b) Alternatively, if sedimentary electron donors (e.g., C_{org})

962 contributed to pore-water anoxia, some fraction of the delivered Fe_{ox} would be reduced to
963 Fe^{2+}, and any P bound to these Fe_{ox} particles would be released to pore-waters. To
964 maintain the low Fe^{2+} loss fraction defining this scenario, any Fe^{2+} ions produced must be
965 captured quantitatively within authigenic ferrous iron minerals. In this instance,
966 sedimentary Fe would be partitioned amongst Fe_{ox}, Fe_{carb}, and Fe_{py} phases, and the
967 dominance of the latter two minerals would imply that much of the original Fe_{ox} flux was
968 reduced. Notably, with regard to P delivery, either scenario for high Fe_{ox} delivery relative
969 to Fe^{2+} loss predicts that the measurement of sedimentary Fe_{HR} represents a close
970 approximation of the magnitude of P delivery associated with the Fe-P shuttle ($\hat{P}^{*}_{Fe}$). If,
971 for example, the Fe cycle were operating in this manner at the time of deposition of the
972 middle and upper Thorntonia members then, under the above assumptions, the Fe-shuttle
973 would be constrained to have contributed a median of ~10% P_T (as determined from Eqn.
974 13) and, therefore, could not represent a dominant source of P for the observed
975 enrichment.

976 If scenarios 1a and 1b cannot source significant amounts of Fe-bound P to
977 phosphatic lithologies, can scenario 2? Like scenario (1b) above, scenario (2) necessitates
978 a redox environment that facilitates the reductive dissolution of the majority of Fe_{ox}
979 delivered to the sediment column, regardless of the size of this flux. In contrast, scenario
980 (2) is distinguished from scenario (1) by the condition that the majority of the
981 sedimentary Fe^{2+} produced must escape to the overlying water column, resulting in less
982 capture of Fe^{2+} ions in authigenic minerals. Such diffusive loss requires anoxia within the
983 water-mass overlying the sediment column. As above, Fe retained within the sediment
984 can reside in any combination of Fe_{ox}, Fe_{carb}, and/or Fe_{py} phases. Notably, Scenario (2)

allows for the measured Fe_{HR} value to significantly underestimate iron oxide delivery to the sea floor ($\hat{Fe}^{*}_{ox}$) and, therefore, to underestimate the Fe-P shuttle ($\hat{P}^{*}_{Fe}$). If, for example, the Fe cycle were operating with an extensive benthic flux of Fe^{2+} to the water column during deposition of the middle Thorntonia Limestone, and if a mechanism existed to preferentially retain the delivered P, then the Fe-P shuttle could have provided a significant proportion of the observed P to these phosphatic strata, that is, greater than the ~10% estimated from Eqn. (13).

In summary, simple models of Fe-bound P delivery estimates ($\hat{P}^{*}_{Fe}$), as determined from Eqn. (13), indicate that this delivery shuttle could have sourced the measured P content of the Arthur Creek Formation. In contrast, our estimates of Fe-bound P can only account for a median of 10% of the P content the Thorntonia Limestone. (This estimate assumes that Fe_{HR} in Thorntonia rocks reflects deposition from the water column. To the extent that Thorntonia iron minerals reflect open-system diagenesis, this estimate would be even lower.) Only by invoking a major diffusive loss of iron from the Thorntonia sediment column with subsequent capture of delivered P within authigenic phases—a scenario for which we do not advocate, yet do not find inconsistent with the assumption of limited diagenesis—could Fe-bound P have provided a more substantial contribution to phosphatic carbonates of the Thorntonia Limestone.

CONCLUSIONS

Within drill core NTGS 99/1, phosphorus enrichment is confined to the middle and upper members of the Thorntonia Limestone, and petrographic observations reveal that this enrichment reflects authigenic apatite mineral nucleation primarily associated

1008 with the interior of bioclasts and, more rarely, as cement in bioclastic grainstone. Under
1009 the canonical model that phosphorus bound within organic matter represents the only
1010 significant delivery flux of phosphorus to the sediment column, molar C_{org}:P_T well below
1011 the Redfield ratio requires significant C_{org} loss or a second delivery source of phosphorus
1012 to Thorntonia sediments.

1013 Interpreted together, sedimentological observations and iron speciation data
1014 suggest that sediment within the southern Georgina Basin accumulated under anoxic,
1015 ferruginous conditions. This redox diagnosis is consistent with previous research
1016 documenting the propensity for anoxic, ferruginous conditions in subsurface water
1017 masses of late Neoproterozoic and Cambrian oceans (Canfield et al., 2008) driven by the
1018 relative fluxes of electron donors (organic carbon) and electron acceptors (reactive Fe,
1019 sulfate) into a basin (Johnston et al., 2010). If correct, the conclusion of an active iron
1020 redox cycle contemporaneous with the deposition of the Thorntonia Limestone and
1021 Arthur Creek Formation provides a second mechanism for augmented sedimentary
1022 phosphorus delivery—phosphorus adsorbed to particulate iron minerals.

1023 The stoichiometries of delivery estimates and remineralization reactions indicate
1024 that the phosphorus content of the Arthur Creek Formation is easily accounted for by any
1025 combination of phosphorus associated with organic matter and/or iron oxide fluxes.
1026 However, the observed phosphorus content of the Thorntonia is difficult to reconcile with
1027 reasonable fluxes of either organic-bound or iron-bound phosphorus alone. Thus, we
1028 suggest that both sources were necessary to account for Thorntonia Limestone phosphatic
1029 carbonate deposition.

The discontinuous nature of phosphorite and phosphatic carbonate through Earth history speaks to discontinuous mechanisms of formation. We hypothesize that redox-mediated phosphorus delivery via the Fe-P shuttle, rather than a discontinuous organic carbon flux, provides the more intermittent mechanism for phosphorus delivery to the sediment column. That said, ferruginous bottom waters appear to have been widespread in Proterozoic oceans, whereas phosphatic carbonates are not. Thus, the episodic nature of phosphate deposition must additionally depend on the fate of phosphate after it enters the sediment column. Where the oxic-anoxic interface lies well within the water column, microbial reduction of ferric iron within the sediments will remobilize P, with a high probability of escape back to the water column. Where phosphate in solution is trapped by skeletons, however, or bound to decay-resistant materials such as chitinous exoskeletons, mineral phosphate may be reprecipitated in sediments. With this in mind, it would appear that delivery mechanisms, post-delivery fate within sediments, and evolution all contributed to the observed geological record of Cambrian phosphate accumulation.

ACKNOWLEDGMENTS

We thank the Northern Territory Geological Survey and Max Heckenberg and Jay Carter of the Alice Springs Core Library for generous access to core material. The Agouron Institute and the NASA Astrobiology Institute (MIT node) provided financial support. We thank Paul Myrow for discussions of sedimentology, Eric Morrow for assistance with data analysis, Greg Eischeid for technical support in the Harvard University Laboratory for Geochemical Oceanography, and David Fike and an anonymous reviewer for critical comments that helped to improve this paper.

REFEENCES CITED

Algeo, T.J., and Ingall, E., 2007, Sedimentary C_{org}:P ratios, paleocean ventilation, and Phanerozoic atmospheric pO_2: Palaeogeography, Palaeoclimatology, Palaeoecology v. p. 130–155, doi.10.1016/j.palaeo.2007.02.029.

Ambrose, G., and Putnam, P., 2006, The Georgina Basin 2006: Northern Territory of Australia onshore hydrocarbon potential: Northern Territory Geological Survey, Record 2006-003.

Ambrose G.J., Kruse P.D., and Putman P.E., 2001, Geology and hydrocarbon potential of the southern Georgina Basin, Australia: Australian Petroleum Production and Exploration Association Journal, v. 41, p. 139–163.

Anderson L. D., Delaney M. L. and Faul K. L., 2001, Carbon to phosphorus ratios in sediments: implications for nutrient cycling: Global Biogeochemical Cycles, v. 15, p. 65–79, doi:10.1029/2000GB001270.

Anderson, T.F., and Raiswell, R., Sources and mechanisms for the enrichment of highly reactive iron in euxinic Black Sea sediments: American Journal of Science, v. 304, p. 203-233, doi:10.2475/ajs.304.3.203.

Babcock, L.E., and Shanchi Peng, 2007, Cambrian chronostratigraphy: Current state and future plans: Palaeogeography, Palaeoclimatology, Palaeoecology, v. 254, p. 62–66, doi:10.1016/j.palaeo.2007.03.011.

Bartley, J.K., Pope, M., Knoll, A.H., Semikhatov, M.A., and Petrov, P.Yu., 1998, A Vendian—Cambrian boundary succession from the northwestern margin of the Siberian Platform: stratigraphy, palaeontology, chemostratigraphy and correlation: Geological Magazine, v. 135, p. 473-494, doi:10.1017/S0016756898008772.

Baturin, G. N., and Bezrukov, P. L., 1979, Phosphorites on the sea floor and their origin: Marine Geology, v. 31, p. 317–332, doi: 10.1016/0025-3227(79)90040-9.

Bengtson, S., and Yue Zhao, 1997, Fossilized metazoan embryos from the earliest Cambrian: Science, v. 277, p. 1645-1648, doi:10.1126/science.277.5332.1645.

Bengtson, S., Conway Morris, S., Cooper, B.J., Jell, P.A., and Runnegar, B.N., 1990, Early Cambrian Fossils from South Australia: Memoirs of the Association of Australasian Palaeontologists, v. 9, p. 1-364.

Benitez-Nelson, C.R., 2000, The biogeochemical cycling of phosphorus in marine systems: Earth-Science Reviews, v. 51, p. 109-135, doi: 10.1016/S0012-82252(00)00018-0.

1099 Bergman, N.M., Lenton, T.M., and Watson, A.J., 2004, COPSE: A new model of
1100 biogeochemical cycling over Phanerozoic time: American Journal of Science, v. 304, p.
1101 397-437, doi: 10.2475/ajs.304.5.397.
1102
1103 Berner, R. A., 1973, Phosphate removal from sea water by adsorption on volcanogenic
1104 ferric oxides: Earth and Planetary Science Letters, v. 18, p. 77–86, doi: 10.1016/0012-
1105 821X(73)90037-X.
1106
1107 Berner, R.A., 2006, GEOCARBSULF: A combined model for Phanerozoic atmospheric
1108 O_2 and CO_2: Geochimica et a Cosmochimica Acta, v. 70, p. 5653-5664, doi:
1109 10.1016/j.gca.2005.11.032.
1110
1111 Bjerrum, C.J., and Canfield, D.E., 2002, Ocean productivity before about 1.9 Gyr ago
1112 limited by phosphorus adsorption onto iron oxides: Nature, v. 417 p. 159–162,
1113 doi:10.1038/417159a.
1114
1115 Boreham, C.J., and Ambrose, G.J., 2005, Cambrian petroleum systems in the southern
1116 Georgina Basin, Northern Territory, Australia, Central Australian Basins Symposium:
1117 petroleum and minerals potential, Alice Springs, NT, 16–18 August 2005.
1118
1119 Brewer, P.G., and Murray, J.W., 1973, Carbon, nitrogen and phosphorus in the Black
1120 Sea: Deep-Sea Research, v. 20, p. 803-818.
1121
1122 Brasier, M.D., and Callow, R.H.T., 2007, Changes in the Patterns of Phosphatic
1123 Preservation across the Proterozoic-Cambrian Transition: Memoirs of the Association of
1124 Australasian Palaeontologists, No. 34, p. 377-389.
1125
1126 Butterfield, N.J., 2003, Exceptional fossil preservation and the Cambrian explosion:
1127 Integrative and Comparative Biology, v. 43, p. 166–177, doi: 10.1093/icb/43.1.166.
1128
1129 Canfield, D.E., 1994, Factors influencing organic carbon preservation in marine
1130 sediments: Chemical Geology, v. 114 p. 315–329, doi: 10.1016/0009-2541(94)90061-2.
1131
1132 Canfield, D.E., Lyons, T.W., and Raiswell, R., 1996, A model for iron deposition to
1133 euxinic Black Sea sediments: American Journal of Science, v. 296, p. 818–834.
1134
1135 Canfield, D.E., Poulton, S.W., Knoll, A.H., Narbonne, G.M., Ross, G., Goldberg, T., and
1136 Strauss, H., 2008, Ferruginous conditions dominated later Neoproterozoic deep-water
1137 chemistry: Science, v. 321, p. 949-952, doi: 10.1126/science.1154499.
1138
1139 Canfield D. E., Raiswell R. and Bottrell S., 1992, The reactivity of sedimentary iron
1140 minerals towards sulfide: American Journal of Science v. 292, p. 659– 683.Canfield D. E.,
1141 Raiswell R., Westrich J. T., Reaves C. M. and Berner R. A., 1986, The use of chromium
1142 reduction in the analysis of reduced inorganic sulfur in sediments and shales: Chemical
1143 Geology, v. 54, p., 149–155, doi: 10.1016/0009-2541(86)90078-1.
1144

1145 Clark, L.L., Ingall, E.D., and Benner, R., 1998, Marine phosphorus is selectively
1146 remineralized: Nature, v. 393, p. 426-426 doi:10.1038/30881.
1147
1148 Cook, P.J., 1992, Phosphogenesis around the Proterozoic-Phanerozoic transition: Journal
1149 of the Geological Society of London, v. 149, p. 615-620, doi: 10.1144/gsjgs.149.4.0615
1150
1151 Cook, P.J., and McElhinny, M.W., 1979, A re-evaluation of the spatial and temporal
1152 distribution of sedimentary phosphate deposits in the light of plate tectonics: Economic
1153 Geology and the Bulletin of the Society of Economic Geologists, v. 74, p. 315–330, doi:
1154 10.2113/gsecongeo.74.2.315.
1155
1156 Cook, P., and Shergold, J.H., 1984, Phosphorus, phosphorites and skeletal evolution at
1157 the Precambrian–Cambrian boundary: Nature v.10, p. 231–236, doi: 10.1038/308231a0.
1158
1159 Cook, P.J., and Shergold, J.H., 1986, Proterozoic and Cambrian phosphorites – nature
1160 and origin: *in* Cook, P.J., and Shergold, J.H., eds., Phosphate deposits of the word:
1161 Proterozoic and Cambrian phosphorites, Volume 1: Cambridge, UK, Cambridge
1162 University Press, p. 369-386.
1163
1164 Cook, P.J., Shergold, J.H., Burnett, W.C., and Riggs, S.R., 1990, Phosphorite research: a
1165 historical overview: Geological Society, London, Special Publication, v. 52, p. 1-22, doi:
1166 10.1144/GSL.SP.1990.052.01.02.
1167
1168 Cordell, D., Drangert, J.-O., and White, S., 2009, The story of phosphorus: Global food
1169 security and food for thought: Global Environmental Change, v. 19, p. 292-305, doi:
1170 10.1016/j.gloenvcha.2008.10.009.
1171
1172 Crowe, S.A., O'Neill, A.H., Katsev, S., Hehanussa, P., Haffner, G.D., Sundby, B., Mucci,
1173 A. and Fowle, D.A., 2008, The biogeochemistry of tropical lakes: a case study from Lake
1174 Matano, Indonesia: Limnology and Oceanography, v. 53, p. 319-331.
1175
1176 Dahl, T.W., Hammarlund, E.U., Anbar, A.D., Bond, D.P.G., Gill, B.C., Gordon, G.W.,
1177 Knoll, A.H., Nielsen, A.T., Schovsbo, N.H., Canfield, D.E., 2010, Devonian rise in
1178 atmospheric oxygen correlated to the radiations of terrestrial plants and large predatory
1179 fish, v. 107, p. 17911-17915, doi: 10.1073/pnas.1011287107.
1180
1181 Delaney M.L., 1998, Phosphorus accumulation in marine sediments and the oceanic
1182 phosphorus cycle: Global Biogeochemical Cycles, v. 12, p. 563–572,
1183 doi:10.1029/98GB02263.
1184
1185 Dellwig, O., Leipe, T., März, C., Glockzin, M., Pollehne, F., Schnetger, B., Yakushev,
1186 E.V., Böttcher, M.E., and Brumsack, H.-J., 2010, A new particulate Mn-Fe-P-shuttle at
1187 the redoxcline of anoxic basins: Geochimica et Cosmochimica Acta, v. 74, p. 7100-7115.
1188
1189 Donoghue, P., Kouchinsky, A., Waloszek, D., Bengtson, S., Dong, X.-p., Val'kov, A.K.,
1190 Cunningham, J.A., and Repetski, J.E., 2006, Fossilized embryos are widespread but the

record is temporally and taxonomically biased: Evolution & Development, v. 8, p. 232–238, doi: 10.1111/j.1525-142X.2006.00093.x.

Dornbos, S.Q., Botjer, D.J., Chen, J.-Y., Gao, F., Oliveri, P., and Li, C.-W., 2006, Environmental controls on the taphonomy of phosphatized animals and animal embryos from the Neoproterozoic Doushantuo Formation, southwest China: Palaios, v. 21, p. 3-14, doi: 10.2110/palo.2004.p04-37.

Dunster, J.N., Kruse, P.D., Duffett, M.L., and Ambrose, G.J., 2007, Geology and resource potential of the southern Georgina Basin: Northern Territory Geological Survey, Digital Information Package DIP007.

Feely, R.A., Trefry, J.H., Massoth, G.J., and Metz, S., 1991, A comparison of the scavenging of phosphorus and arsenic from seawater by hydrothermal iron oxyhydroxides in the Atlantic and Pacific Oceans: Deep Sea Research, v. 38, p., 617-623, doi: 10.1016/0198-0149(91)90001-V.

Feely, R.A., Trefry, J.H., Lebon, G.T., and German, C.R., 1998, The relationship between P/Fe and V/Fe ratios in hydrothermal precipitates and dissolved phosphate in seawater: Geophysical Research Letters, v. 25, p. 2253-2256, doi:10.1029/98GL01546.

Filippelli, G.M., 2011, Phosphate rock formation and marine phosphorus geochemistry: the deep time perspective: Chemosphere, v. 84, p. 759-766, doi: 10.1016/j.chemosphere.2011.02.019.

Filippelli, G.M., and Delaney, M.L., 1992, Similar phosphorus fluxes in ancient phosphorite deposits and a modern phosphogenic environment: Geology, v. 20, p. 709-712, doi: 10.1130/0091-7613(1992)020<070.

Föllmi, K.B., 1996, The phosphorus cycle, phosphogenesis and marine phosphate-rich deposits: Earth-Science Reviews, v. 40, p. 55–124, doi: 10.1016/0012-8252(95)00049-6.

Föllmi, K.B., Badertscher, C., de Kaenel, E., Stille, P., John, C. M., Adatte, T., and Steinmann, P, 2005), Phosphogenesis and organic-carbon preservation in the Miocene Monterey Formation at Naples Beach, California—The Monterey hypothesis revisited: Geological Society of America Bulletin, v. 117, p. 589-619, doi:10.1130/B25524.1.

Garrels, R.M., and Lerman, A., 1984, Coupling of the sedimentary sulfur and carbon cycles; an improved model: American Journal of Science, v. 284, p. 989-1007, doi: 10.2475/ajs.284.9.989.

Geider, R., and La Roche, J., 2002, Redfield revisited: variability of C:N:P in marine microalgae and its biochemical basis: European Journal of Phycology, v. 37, p. 1-17, doi:10.1017/S0967026201003456.

German, C.R., Klinkhammer, G.P., Edmond, J.M., Mitra, A., and Elderfield, H., 1990,

1237 Hydrothermal scavenging of rare earth elements in the ocean: Nature, v. 345, p. 516–518,
1238 doi:10.1038/345516a0.

1239 Gomez, F.J., Ogle, N., Astini, R.A., and Kalin, R.M., 2007, Paleoenvironmental and
1240 Carbon-Oxygen Isotope Record of Middle Cambrian Carbonates (La Laja Formation) in
1241 the Argentine Precordillera: Journal of Sedimentary Research, v. 77, p. 826-842, doi:
1242 10.2110/jsr.2007.079.

1243 Guo, H., Du, Y., Kah, L.C., Huang, J., Hu, C., Huang, H. and Yau, W., 2013, Isotopic
1244 composition of organic and inorganic carbon from the Mesoproterozoic Jixian Group,
1245 North China: Implications for biological and oceanic evolution: Precambrian Research, v.
1246 224, p. 169-183, doi: 10.1016/j.precamres.2012.09.023.

1247 Guo, Q., Strauss, H., Liu, C., Zhao, Y., Yang, X., Peng, J., and Yang, H., 2010, A
1248 negative carbon isotope excursion defines the boundary from Cambrian Series 2 to
1249 Cambrian Series 3 on the Yangtze Platform, South China: Palaeogeography,
1250 Palaeoclimatology, Palaeoecology, v. 285, p. 143–151, doi:10.1016/j.palaeo.2009.11.005.

1251 Howard, P.F., 1990, The distribution of phosphatic facies in the Georgina, Wiso and Daly
1252 River Basins, Northern Australia: Geological Society, London, Special Publications, v.
1253 52, p. 261-272, doi: 10.1144/GSL.SP.1990.052.01.19

1254 Hedges, J.I., and Kiel, R.G., 1995, Sedimentary organic matter preservation: an
1255 assessment and speculative synthesis: Marine Chemistry, v. 49, p.81-115, doi:
1256 10.1016/0304-4203(95)00008-F.

1257 Holland, H.D., 2006, The oxygenation of the atmosphere and oceans: Philosophical
1258 Transactions of the Royal Society–B, v. 361, p. 903-915, doi: 10.1098/rstb.2006.1838.
1259
1260 Ingall, E.D., Bustin, R.M., and Van Cappellen, P., 1993, Influences of water column
1261 anoxia on the burial and preservation of carbon and phosphorus in marine shales:
1262 Geochimica et Cosmochimica Acta, v. 57, p. 303–316, doi: 10.1016/0016-
1263 7037(93)90433-W.
1264
1265 Ingall E. D. and Jahnke R. A., 1997, Influence of water- column anoxia on the elemental
1266 fractionation of carbon and phosphorus during sediment diagenesis: Marine Geology, v.
1267 139, p. 219–229, doi: 10.1016/S0025-3227(96)00112-0.
1268
1269 Jilbert, T., and Slomp, C.P., 2013, Iron and manganese shuttles control the formation of
1270 authigenic phosphorus minerals in the euxinic basins of the Baltic Sea: Geochimica et
1271 Cosmochimica Acta, v. 107, p. 155-169, doi: 10.1016/j.gca.2013.01.005.
1272
1273 Jilbert, T., Slomp, C.P., Gustafsson, B.G., and Boer, W., 2011, Beyond the Fe-P-redox
1274 connection: preferential regeneration of phosphorus from organic matter as a key control
1275 on Baltic Sea nutrient cycles: Biogeosciences, v. 8, p. 1699-1720, doi: 10.5194/bg-8-
1276 1699-2011.
1277

1278 Johnston, D.T., Poulton, S.W., Dehler, C., Porter, S., Husson, J., Canfield, D.E., and
1279 Knoll, A.H., 2010, An emerging picture of Neoproterozoic ocean chemistry: Insights
1280 from the Chuar Group, Grand Canyon, USA: Earth and Planetary Science Letters, v. 290,
1281 p. 64-73, doi: 10.1016/j.epsl.2009.11.059.
1282
1283 Kappler, A., and Newman, D.K., 2004, Formation of Fe(III)-minerals by Fe(II)-
1284 oxidizing photoautotrophic bacteria: Geochimica et Cosmochimica Acta, v. 68, p. 1217–
1285 1226, doi:10.1016/j.gca.2003.09.006.

1286 Kazakov, A.V., 1937, The phosphate facies: Origin of phosphorites and geological
1287 factors of deposit formation: Proceedings of the Scientific Institute of Fertilizers and
1288 Insectofungicides, v. 145, p. 1–106.
1289
1290 Konhauser, K.O., 2007, Introduction to Geomicrobiology: Oxford, Blackwell Science,
1291 425 p.
1292
1293 Konhauser, K.O., Lalonde, S.V., Amskold, L., and Holland, H.D., 2007, Was There
1294 Really an Archean Phosphate Crisis?: Science, v. 315, p. 1234, doi:
1295 10.1126/science.1136328.

1296 Kouchinsky, A., Bengtson, S., Runnegar, B., Skovsted, C., Steiner, M., and Vendrasco,
1297 M., 2012, Chronology of early Cambrian biomineralization: Geological Magazine, v.
1298 149, p. 221-251, doi: 10.1017/S0016756811000720.
1299
1300 Krom, M.D., and Berner, R.A., 1981, The diagenesis of phosphorus in a nearshore
1301 marine sediment: Geochimica et Cosmochimica Acta, v. 45, p. 207–216, doi:
1302 10.1016/0016-7037(81)90164-2.
1303
1304 Laurie, J.R., 2004a, Early Middle Cambrian trilobites from Pacific Oil & Gas Baldwin 1
1305 well, southern Georgina Basin, Northern Territory: Memoirs of the Association of
1306 Australasian Palaeontologists v. 32, p. 127-204.
1307
1308 Laurie, J.R., 2004b, Early Middle Cambrian trilobite faunas from NTGS Elkedra 3
1309 corehole, southern Georgina Basin, Northern Territory: Memoirs of the Association of
1310 Australasian Palaeontologists, v. 30, p. 221-260.
1311
1312 Lindsay, J.F., 2002, Supersequences, superbasins, supercontinents – evidence from the
1313 Neoproterozoic–Early Palaeozoic basins of central Australia: Basin Research, v. 14, p.
1314 207-223, doi: 10.1046/j.1365-2117.2002.00170.x.
1315
1316 Lindsay, J.F., Kruse, P.D., Green, O.R., Hawkins, E., Brasier, M.D., Cartlidge, J., and
1317 Corfield, R.M., 2005, The Neoproterozoic–Cambrian record in Australia: a stable isotope
1318 study: Precambrian Research, v. 143, p. 113–133, doi: 10.1016/j.precamres.2005.10.002.
1319
1320 Lyons, T.W., and Severmann, S., 2006, A critical look at iron paleoredox proxies: New
1321 insights from modern euxinic marine basins: Geochimica et Cosmochimica Acta, v. 70,
1322 p. 5698–5722, doi: 10.1016/j.gca.2006.08.021.

Martin, J.-M., and Meybeck, M., 1979, Elemental mass-balance of material carried by major world rivers: Marine Chemistry, v. 7. P. 173-206, doi:10.1016/0304-4203(79)90039-2.

März, C., Poulton, S.W., Beckmann, B., Küster, K., Wagner, T., and Kasten, S., 2008, Redox sensitivity of P cycling during marine black shale formation: Dynamics of sulfidic and anoxic, non-sulfidic bottom waters: Geochimica et Cosmochimica Acta, v. 72, p. 3703–3717, doi: 10.1016/j.gca.2008.04.025.

Mayer, T.D., and Jarrell, W.M., 2000, Phosphorus sorption during iron(III) oxidation in the presence of dissolved silica: Water Research, v. 34, p. 3949-3956, doi:10.1016/S0043-1354(00)00158-5.

Olivarez, A.M., and Owen, R.M., 1989, REE/Fe variations in hydrothermal sediments: Implications for the REE content of seawater: Geochimica et Cosmochimica Acta, v. 53, p. 757–762, doi:10.1016/0016-7037(89)90019-7.

Papineau, D., 2010, Global biogeochemical changes at both ends of the Proterozoic: Insights from phosphorites: Astrobiology, v. 10, p. 165–181, doi:10.1089/ast.2009.0360.

Peng, Shanchi, and Babcock, L.E., 2011, Continuing progress on chronostratigraphic subdivision of the Cambrian System: Bulletin of Geosciences, doi: 10.3140/bull.geosci.1273.

Planavsky, N.J., Rouxel, O.J., Bekker, A., Lalonde, S.V., Konhauser, K.O., Reinhard, C.T., and Lyons, T.W., 2010, The evolution of the marine phosphate reservoir: Nature, v. 467, p. 1088–1090, doi:10.1038/nature09485

Porter, S.M., 2004a, Halkieriids in Middle Cambrian phosphatic limestones from Australia: Journal of Paleontology, v. 78, p. 574–590, doi: 10.1666/0022-3360(2004)078<0574:HIMCPL>2.0.CO;2.

Porter, S.M., 2004b, Closing the phosphatization window: testing for the influence of taphonomic megabias on the pattern of small shelly fossil decline: Palaios, v. 19, p. 178–183, doi: 10.1669/0883-1351(2004)019<0178.

Poulton, S.W., and Canfield, D.E., 2005, Development of a sequential extraction procedure for iron: implications for iron partitioning in continentally derived particulates: Chemical Geology, v. 214, p. 209–221, doi: 10.1016/j.chemgeo.2004.09.003.

Poulton, S.W., and Canfield, D. E., 2006, Co-diagenesis of iron and phosphorus in hydrothermal sediments from the southern East Pacific rise: implications for the evaluation of paleoseawater phosphate concentrations: Geochimica et Cosmochimica Acta, v. 70, p. 5883–5898, doi: 10.1016/j.gca.2006.01.031.

1368 Poulton, S.W., and Canfield, D.E., 2011, Ferruginous Conditions: A Dominant Feature of
1369 the Ocean through Earth's History: Elements, v. 7, p. 107-112,
1370 doi:10.2113/gselements.7.2.107.
1371
1372 Poulton S. W., and Raiswell R., 2002, The low-temperature geochemical cycle of iron:
1373 from continental fluxes to marine sediment deposition: American Journal of Science, v.
1374 302, p. 774–805, doi: 10.2475/ajs.302.9.774.
1375
1376 Poulton S. W., Fralick, P.W., and Canfield, D.E., 2004, The transition to a sulphidic
1377 ocean ~ 1.84 billion years ago: Nature, v. 431, p. 173-177, doi:10.1038/nature02912.
1378
1379 Raiswell, R., and Berner, R.A., 1987, Organic carbon losses during burial and thermal
1380 maturation of normal marine shales: Geology, v. 15, p. 853-856, doi: doi: 10.1130/0091-
1381 7613(1987)15<853:OCLDBA>2.0.CO;2.
1382
1383 Raiswell, R., and Canfield, D.E., 1998, Sources of iron for pyrite formation in marine
1384 sediments: American Journal of Science, v. 298, p. 219–245, doi: 10.2475/ajs.298.3.219.
1385
1386 Raiswell, R., Newton, R.J., and Wignall, P.B., 2001, An indicator of water-column
1387 anoxia: resolution of biofacies variations in the Kimmeridge Clay (Upper Jurassic, U.K.):
1388 Journal of Sedimentary Research, v. 71, p. 286–294, doi: 10.1306/070300710286.
1389
1390 Randall, S.R., Sherman, D.M., and Vala Ragnarsdottir, K., 2001, Sorption of As(V) on
1391 green rust (Fe4(II)Fe2(III)(OH)12SO4•3H2O) and lepidocrocite (γ-FeOOH): Surface
1392 complexes from EXAFS spectroscopy: Geochimica et Cosmochimica Acta, v. 65, p.
1393 1015–1023, doi:10.1016/S0016-7037(00)00593-7.

1394 Redfield, A.C., 1958, The biological control of chemical factors in the environment:
1395 American Scientist, v. 64, p. 205-221.

1396 Riggs, S.R., 1986, Proterozoic and Cambrian phosphorites – specialist studies:
1397 phosphogenesis and its relationship to exploration for Proterozoic and Cambrian
1398 phosphorites: in Cook, P.J., and Shergold, J.H., eds., Phosphate deposits of the word:
1399 Proterozoic and Cambrian phosphorites, Volume 1: Cambridge, UK, Cambridge
1400 University Press, p. 352-368.
1401
1402 Ruttenberg, K.C., 1992, Development of a sequential extraction method for different
1403 forms of phosphorus in marine sediments: Limnology and Oceanography, v. 37, p. 1460–
1404 1482, doi: 10.4319/lo.1992.37.7.1460.
1405
1406 Ruttenberg, K.C., and Berner, R.A., 1993, Authigenic apatite formation and burial in
1407 sediments from non-upwelling, continental margin environments: Geochimica et
1408 Cosmochimica Acta, v. 57, p. 991-1007.
1409
1410 Saltzman, M.R., 2005, Phosphorus, nitrogen, and the redox evolution of the Paleozoic
1411 oceans: Geology v. 33, p. 573–576, doi: 10.1130/G21535.1.
1412

1413 Schrag, D.P., Higgins, J.A., Macdonald, F.A., and Johnston, D.T., 2013, Authigenic
1414 carbonate and the history of the global carbon cycle: Science, v. 339, p. 540-543, doi:
1415 10.1126/science.1229578.
1416
1417 Schuffert, J.D., Jahnke, R.A., Kastner, M., Leather, J., Sturz, A., and Wing, M.R., 1994,
1418 Rates of formation of modern phosphorite off western Mexico: Geochimica et
1419 Cosmochimica Acta, v. 58, p. 5001–5010, doi: 10.1016/0016-7037(94)90227-5.
1420
1421 Schuffert, J.D., Kastner, M., and Jahnke, R.A., 1998, Carbon and phosphorus burial
1422 associated with modern phosphorite formation: Marine Geology, v. 146, p. 21-31.
1423
1424 Scranton, M.I., McIntyre, M., Astor, Y., Taylor, G.T., Mueller-Karger, F., and Fanning.,
1425 K., 2006, Temporal variability in the nutrient chemistry of the Cariaco Basin: in: Neretin,
1426 L.N. (ed.), Past and Present Water Column Anoxia: Springer Berlin Heidelberg New
1427 York, p. 139-160.
1428
1429 Severmann, S., Lyons, T.W., Anbar, A., McManus, J., and Gordon, G., 2008, Modern
1430 iron isotope perspective on the benthic iron shuttle and the redox evolution of ancient
1431 oceans: Geology, v. 36, p. 487-490, doi: 10.1130/G24670A.1.
1432
1433 Severmann, S., McManus, J., Berelson, W.M., and Hammond, D.E., 2010, The
1434 continental shelf benthic iron flux and its isotopic composition: Geochimica et
1435 Cosmochimica Acta, v. 74, p. 3984-4004, doi: 10.1016/j.gca.2010.04.022.
1436
1437 Shaffer, G., 1986, Phosphate pumps and shuttles in the Black Sea: Nature, v. 321, p. 515-
1438 517, doi:10.1038/321515a0.
1439
1440 Shemesh, A., 1990, Crystallinity and diagenesis of sedimentary apatites: Geochimica et
1441 Cosmochimica Acta, v. 54, p. 2433-2438, doi: 10.1016/0016-7037(90)90230-I.
1442
1443 Shen, Y., Schidlowski, M., and Chu, X., 2000, Biogeochemical approach to
1444 understanding phosphogenic events of the terminal Proterozoic to Cambrian:
1445 Palaeogeography Palaeoclimatology Palaeoecology, v. 158, p. 99–108, doi:
1446 10.1016/S0031-0182(00)00033-X.
1447
1448 Siever, R., 1992, The silica cycle in the Precambrian: Geochimica et Cosmochimica Acta,
1449 v. 56, p. 3265-3272, doi: 10.1016/0016-7037(92)90303-Z.
1450
1451 Slomp, C.P., Epping, E.H.G., Helder, W., and Van Raaphorst, W., 1996, A key role for
1452 iron-bound phosphorus in authigenic apatite formation in North Atlantic continental
1453 platform sediments: Journal of Marine Research, v. 54, p. 1179-1205, doi:
1454 10.1357/0022240963213745.
1455
1456 Slomp C. P., Thomson J., and De Lange G. J., 2004, Controls on phosphorus
1457 regeneration and burial during formation of eastern Mediterranean sapropels: Marine
1458 Geology, v. 203, p. 141–159, doi: 10.1016/S0025-3227(03)00335-9.

Southgate, P.N., 1988, A model for the development of phosphatic and calcareous lithofacies in the Middle Cambrian Thorntonia Limestone, northeast Georgina Basin, Australia: Australian Journal of Earth Sciences, v. 35, p. 111-130, doi: 10.1080/08120098808729443.

Southgate, P.N., and Shergold, J.H., 1991, Application of sequence stratigraphic concepts to Middle Cambrian phosphogenesis, Georgina Basin, Australia: Journal of Australian Geology and Geophysics, v. 12, p. 119–144.

Strickland, J.D.H., and Parsons, T.R., 1972, A Practical Handbook of Seawater Analysis: Fish Research Board of Canada.

Swanson-Hysell, N.L, Rose, C.V., Calmet, C.C., Halverson, G.P., Hurtgen, M.T., and Maloof, A.C., 2010, Cryogenian glaciation and the onset of carbon-isotope decoupling: Science, v. 328, 608-611, doi:10.1126/science.1184508.

Trappe, J., 2001, A nomenclature system for granular phosphate rocks according to depositional texture: Sedimentary Geology, v. 145, p. 135–150, doi: 10.1016/S0037-0738(01)00103-8.

Trefry, J.H., and Metz, S., 1989, Role of hydrothermal precipitates in the geochemical cycling of vanadium: Nature, v. 342, p. 531–533, doi:10.1038/342531a0.

Trocine, R.P., and Trefry, J.H., 1988, Distribution and chemistry of suspended particles from an active hydrothermal vent site on the Mid-Atlantic Ridge at 26°N: Earth and Planetary Science Letters, v. 88, p. 1–15, doi:10.1016/0012-821X(88)90041-6.

Tyrrell, T., 1999, The relative influences of nitrogen and phosphorus on oceanic primary production: Nature v. 400, p.525–531, doi:10.1038/22941.

Van Cappellen, P., and Ingall, E.D., 1996, Redox stabilization of the atmosphere and oceans by phosphorus-limited marine productivity: Science, v. 271, p. 493-496, doi: 10.1126/science.271.5248.493.

Vine, J.D., and Tourtelot, E.B., 1970, Geochemistry of black shale deposits; a summary report: Economic Geology, v. 65 no. 3 p. 253-272, doi: 10.2113/gsecongeo.65.3.253.

Walter, M.R., Veevers, J.J., Calver, C.R., and Grey, K., 1995, Neoproterozoic stratigraphy of the Centralia Superbasin, Australia: Precambrian Research, v. 73, p. 173-195, doi: 10.1016/0301.9268(94)00077-5.

Wang, X., Hu, W., Yao, S., Chen, Q., and Xie, X., 2011, Carbon and strontium isotopes and global correlation of Cambrian Series 2-Series 3 carbonate rocks in the Keping area of the northwestern Tarim Basin, NW China: Marine an Petroleum Geology, v. 28, p. 992-1002, doi:10.1016/j.marpetgeo.2011.01.006.

1501 Xiao, S. H. and Knoll, A. H., 1999, Fossil preservation in the Neoproterozoic
1502 Doushantuo phosphorite Lagerstatte, South China: Lethaia, v. 32, p. 219 – 240, doi:10.
1503 1111/j.1502-3931.1999.tb00541.x
1504
1505 Xiao, S.H., and Knoll, A.H., 2000, Phosphatized animal embryos from the
1506 Neoproterozoic Doushantuo formation at Weng'an, Guizhou, south China: Journal of
1507 Paleontology v. 74, p. 767–788, doi:10.1666/0022-3360(2000)074,0767:PA
1508 EFTN.2.0.CO;2.
1509
1510 Zegeye, A., Bonneville, S. Benning, L.G., Sturm, A., Fowle, D.A., Jones, C. Canfield,
1511 D.E., Ruby, C., MacLean, L.C, Nomosatryo, S., Crowe, S.A., and Poulton, S.W., 2012,
1512 Green rust formation controls nutrient availability in a ferruginous water column:
1513 Geology, v. 40, p. 599-602, doi:10.1130/G32959.1.

1514 Zhu, M.-Y., Zhang, J.-M., Li, G.-X., and Yang, A.-H., 2004, Evolution of C isotopes in
1515 the Cambrian of China: implications for Cambrian subdivision and trilobite mass
1516 extinctions: Geobios, v. 37, p. 287-301, doi: 10.1016/j.geobios.2003.06.001.

Figure captions:

Figure 1: (A) Areal extent of the constituent basins of the Neoproterozoic Centralian Superbasin. The black dot marks the drill locality for core NTGS 99/1 in the southern Georgina Basin. **(B)** Chronostratigraphy and lithostratigraphic nomenclature for the Northern Territory outcroppings of Cambrian strata within the southern Georgina Basin (modified from Dunster et al., 2007). The symbol "(?)" reflects uncertainties in correlating regional Australian trilobite Zones with International Cambrian System designations.

Figure 2: Lithofacies of the Thorntonia Limestone and Arthur Creek Formation in NTGS 99/1. **(A)** Sandy dolostone of the lower Thorntonia Limestone, just above the contact with the underlying Paleoproterozoic granite basement (~595.8 – 595.6 mcd). **(B)** General character of the mottled-to-stylonodular, dolomitic lower Thorntonia Limestone (584 – 580.5 mcd). **(C)** Characteristic meter to sub-meter scale lithologic alternations and color variation within limestone of the middle Thorntonia Limestone (577.7 – 571.4 mcd). (1) Denotes black and dark gray calcimudstone; (2) denotes lighter gray calcimudstone, wackestone and packstone; and (3) denotes limestone grainstone. Note the general up-package coarsening and lightening, often without cyclic or predictable variation. **(D)** Bioclastic grainstone to mudstone transition from 570.15 – 570.05 mcd (middle Thorntonia Limestone; all limestone). **(E)** Appearance of the vuggy, bioclastic dolomitic grainstone of the upper Thorntonia Limestone (left) and the overlying basal 'hot shale' of the lower Arthur Creek Formation (right). Contact at 554.7 mcd. **(F)** The laminated siliciclastic shale/siltstone and calcimudstone facies of the lower Arthur Creek Formation. **(G)** Light-gray early diagenetic nodule (calcimudstone) displacing dark-gray laminations within the lower Arthur Creek Formation at 532.8 – 532.65 mcd (arrows mark the exterior of the nodule). **(H)** General appearance of the interbedded siliciclastic mudstone/siltstone and calcimudstone (neomorphosed to microspar) facies of the lower Arthur Creek Formation above ~430 mcd.

Figure 3: Photomicrographs under plane-polarized light of authigenic apatite distribution within the middle Thorntonia Limestone. **(A)** A limestone packstone with apatite

replacement specifically targeting the interior of conical small shelly fossil elements at 570.35 mcd. **(B)** Wholesale matrix and grain phosphatization at of a limestone at 575.17 mcd. **(C)** Dispersed, allochthonous grains of authigenic apatite within a limestone at 560.69 mcd (see text for discussion of origin).

Figure 4: Lithology and stable isotope chemostratigraphy of the Thorntonia Limestone and lower Arthur Creek Formation within drill core NTGS 99/1. For all panels, data for the lower and middle/upper Thorntonia Limestone are plotted in open and solid blue circles, respectively, while data for the Arthur Creek Formation are plotted in solid red circles. **(A)** Generalized stratigraphic column depicting the lithology of the lower, middle, and upper Thorntonia Limestone and the lower Arthur Creek Formation. Lithologic abbreviations: Siliciclastics: slts = siltstone; Carbonates: mds = mudstone; wks = wackestone; pks = packstone; grn = grainstone. Vertical axis reflects meters core depth from the surface. **(B)** Carbonate carbon isotopic composition (relative to V-PDB). **(C)** Carbonate oxygen isotopic composition (relative to V-PDB). **(D)** Total organic carbon isotopic composition (symbol size scaled to wt.% total organic carbon (TOC)). **(E)** Cross-plot of carbonate carbon and carbonate oxygen isotopic composition. **(F)** Cross-plot of organic carbon and carbonate carbon isotopic composition.

Figure 5: Phosphorus and iron speciation geochemistry, molar C:P ratios, and correlations between P and other geochemical metrics within the Thorntonia Limestone and Arthur Creek Formation. **(A)** The weight percent of total phosphorus (filled green circles) and subtotal phosphorus (open green circles) for those samples whose P_{Fe} concentrations were not determined from P-speciation geochemistry. Weight percent total Fe (open red circles) from Fe-speciation geochemistry. Note the logarithmic scale to emphasize, in particular, the P content of the middle and upper Thorntonia Limestone. **(B)** The weight percents of operationally-defined phosphorus phases as determined by phosphorus-speciation geochemistry. Note the logarithmic scale. See text for discussion of the operationally-defined P phases. **(C)** The weight percents of iron phases as determined by iron-speciation geochemistry. Note the logarithmic scale. **(D)** The molar ratio of organic carbon to total phosphorus. Grey line intersects the axis at C:P = 106:1,

the canonical Redfield ratio. **(E)** Correlation between the weight percent phosphorus within individual samples as determined from ICP-AES versus that determined by the sequential extraction method (see Methods section). Slope of linear regression = 1.1; R^2 = 0.88. **(F)** Correlation between the zirconium to aluminum ratio (ppm/%) and the operationally-defined P_{xl} phase (see text for discussion) determined from phosphorus speciation geochemistry. **(G)** Cross-plot of the weight percent of highly reactive iron species (Fe_{HR}; oxides, magnetite, pyrite, and iron carbonates) determined from iron-speciation geochemistry versus the weight percent of total phosphorus determined from phosphorous-speciation geochemistry.

Figure 6: Iron-speciation geochemistry. For all panels, data for the lower and middle/upper Thorntonia Limestone are plotted in open and solid blue circles, respectively, while data for the laminated facies and interbedded siliciclastic/carbonate mudstone facies of the Arthur Creek Formation are plotted in solid and open red circles, respectively. Data from the Arthur Creek 'hot shale' appear as solid red circles with a black outline. **(A)** A cross-plot of the weight percent total iron (Fe_T) versus the weight percent iron within highly reactive phases (Fe_{HR}; oxides, magnetite, pyrite, and iron carbonates). We plot slopes of 1 and 0.38 as a reference for comparing these carbonate data to previously published iron-speciation data, but we do not advocate interpreting carbonate data (blue circles) within the canonical siliciclastic framework. Slope of regressions (not plotted) reflect the percentage of the total iron residing in highly reactive phases (lower Thorntonia = 57%, R^2: 0.53; middle/upper Thorntonia = 89%, R^2: 0.95; laminated facies of the Arthur Creek = 53%, R^2: 0.44; interbedded siliciclastic shale / siltstone and carbonate mudstone facies of the Arthur Creek = 26%, R^2: 0.90). **(B)** A cross-plot of the weight percent highly reactive iron (Fe_{HR}) versus the weight percent iron within pyrite (Fe_{py}). We plot slopes of 1 and 0.8 for reference (see (a)). Slope of regressions (not plotted) reflect the percentage of the highly reactive iron residing within pyrite (lower Thorntonia = 17%, R^2: 0.07; middle/upper Thorntonia = 64%, R^2: 0.95; laminated facies of the Arthur Creek = 75%, R^2: 0.95; interbedded siliciclastic shale / siltstone and carbonate mudstone facies of the Arthur Creek = 30%, R^2: 0.50). We note that the linear regression for the 'hot shale' ($Fe_{py} = 0.8*(Fe_{HR})-0.2$) is the same for the

lower Arthur Creek laminated facies exclusive of the 'hot shale' data. **(C)** A cross-plot of the weight percent highly reactive iron (Fe_{HR}) versus iron carbonate (Fe_{carb}). Slope of regressions (not plotted) reflect the percentage of the highly reactive iron residing within iron carbonate (lower Thorntonia = 82%, R^2: 0.62; middle/upper Thorntonia = 31%, R^2: 0.82; laminated facies of the Arthur Creek = 25%, R^2: 0.68; interbedded siliciclastic shale / siltstone and carbonate mudstone facies of the Arthur Creek = 52%, R^2: 0.73). We note that the linear regression for the 'hot shale' ($Fe_{carb} = 0.25*(Fe_{HR})+0.15$) is similar for the lower Arthur Creek laminated facies exclusive of the 'hot shale' data ($Fe_{carb} = 0.20*(Fe_{HR})+0.15$).

Figure 7: Assessing the potential contribution of organic-bound and iron-bound phosphorus (P) to authigenic apatite precipitation. For the case of organic-bound P delivery (left), the dashed boxes depict the median estimated weight percent organic matter (wt.% $\hat{C}^*_{org}$) necessary to account for the measured wt.% sedimentary P based on equation (1) with a Redfield ratio of 106C:1P. Dark grey boxes represent the median wt.% total organic carbon (TOC) measured within samples. Light gray boxes represent the corrected wt.% $\hat{C}^*_{org}$ (see discussion leading to equation (9)). All values plotted to scale. Organic carbon delivery can account for all of the P within the Arthur Creek Formation. In contrast, the blank area within the dashed Thorntonia Limestone box represents the amount of $\hat{C}^*_{org}$ that would have to have been remineralized to account for the observed sedimentary P content if it were sourced by organic-bound P alone.

For the case of iron-bound P delivery (right), the dashed boxes depict the median measured wt.% P_T within samples while the dark grey boxes represent the estimated delivery of iron-bound P ($\hat{P}^*_{Fe}$) as determined from equation (13) assuming a partition coefficient for ferrihydrite and a seawater phosphate concentration of 5 μm (see text for discussion). All values plotted to scale. In this regard, and under these assumptions, the Fe-P delivery shuttle can account for all of the P within the Arthur Creek Formation. In contrast, only by invoking Fe^{2+} loss from the sediment column and preferential capture of Fe-bound P within authigenic phases, could the Fe-P shuttle have contributed more substantially (> ~10%) to the phosphatic carbonate of the Thorntonia Limestone.

Figure 1
Click here to download Figure: NTGS Fig 1.pdf

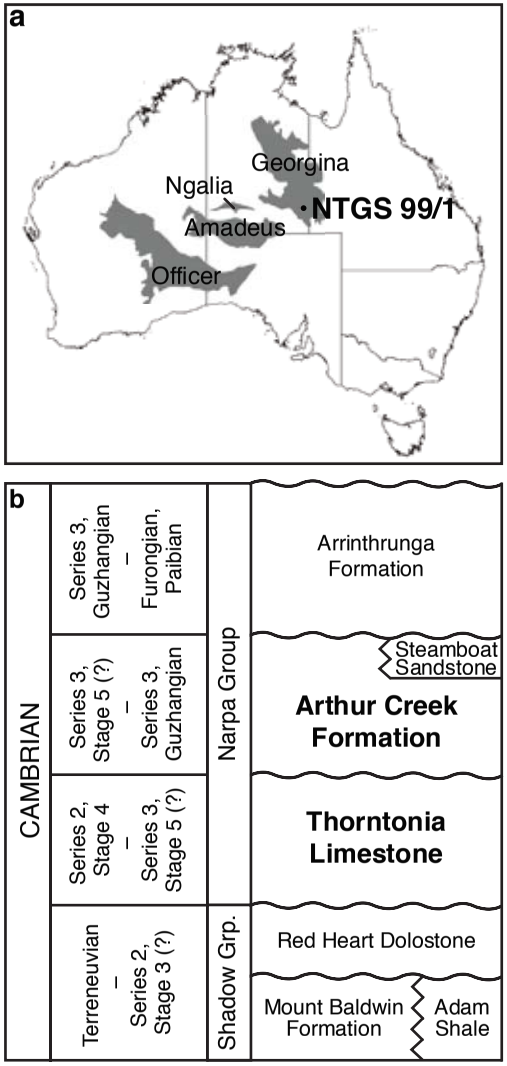

Figure 2
Click here to download Figure: NTGS Fig 2.pdf

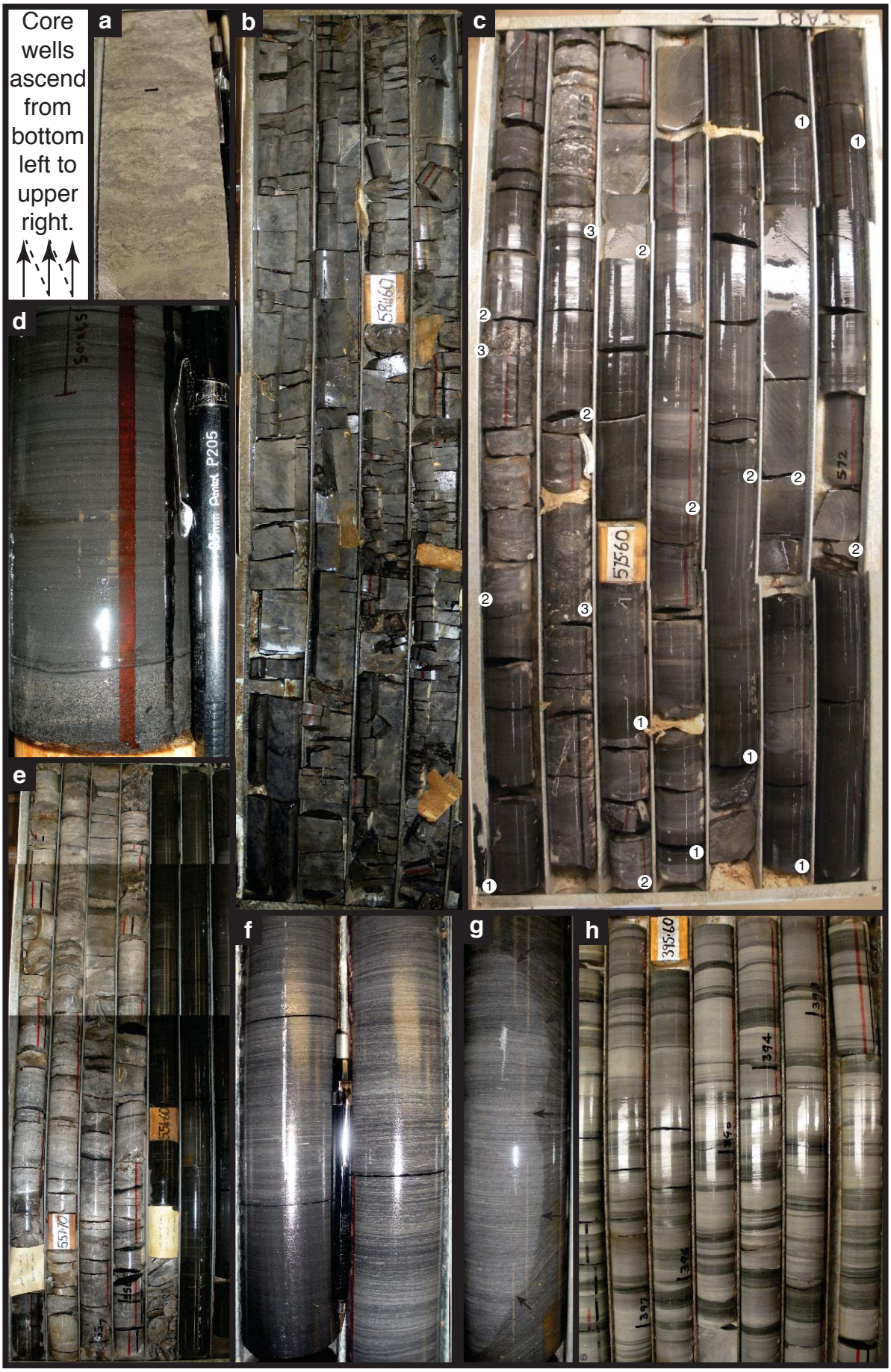

Figure 3
Click here to download Figure: NTGS Fig 3.pdf

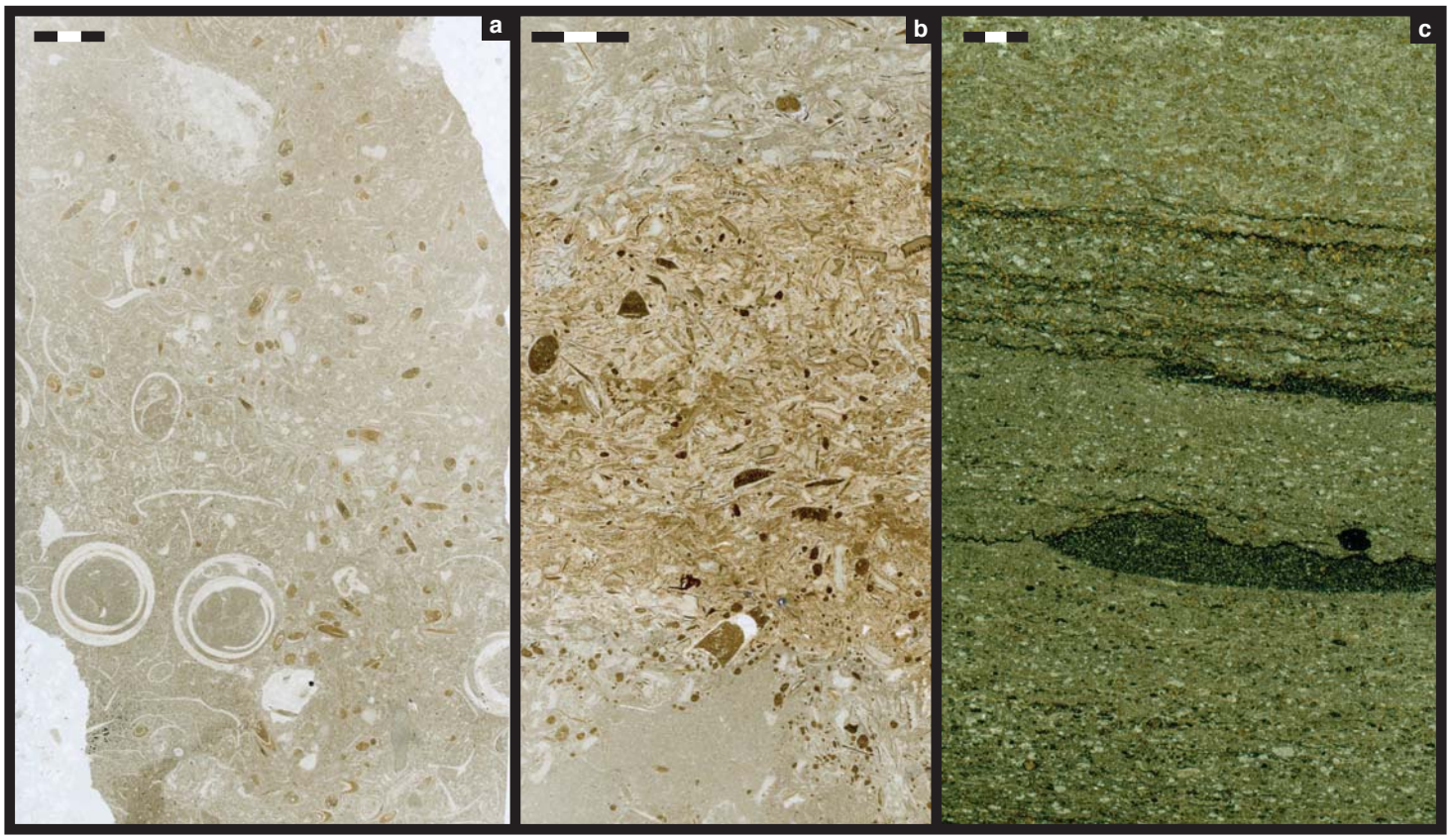

Figure 4
Click here to download Figure: NTGS Fig 4.pdf

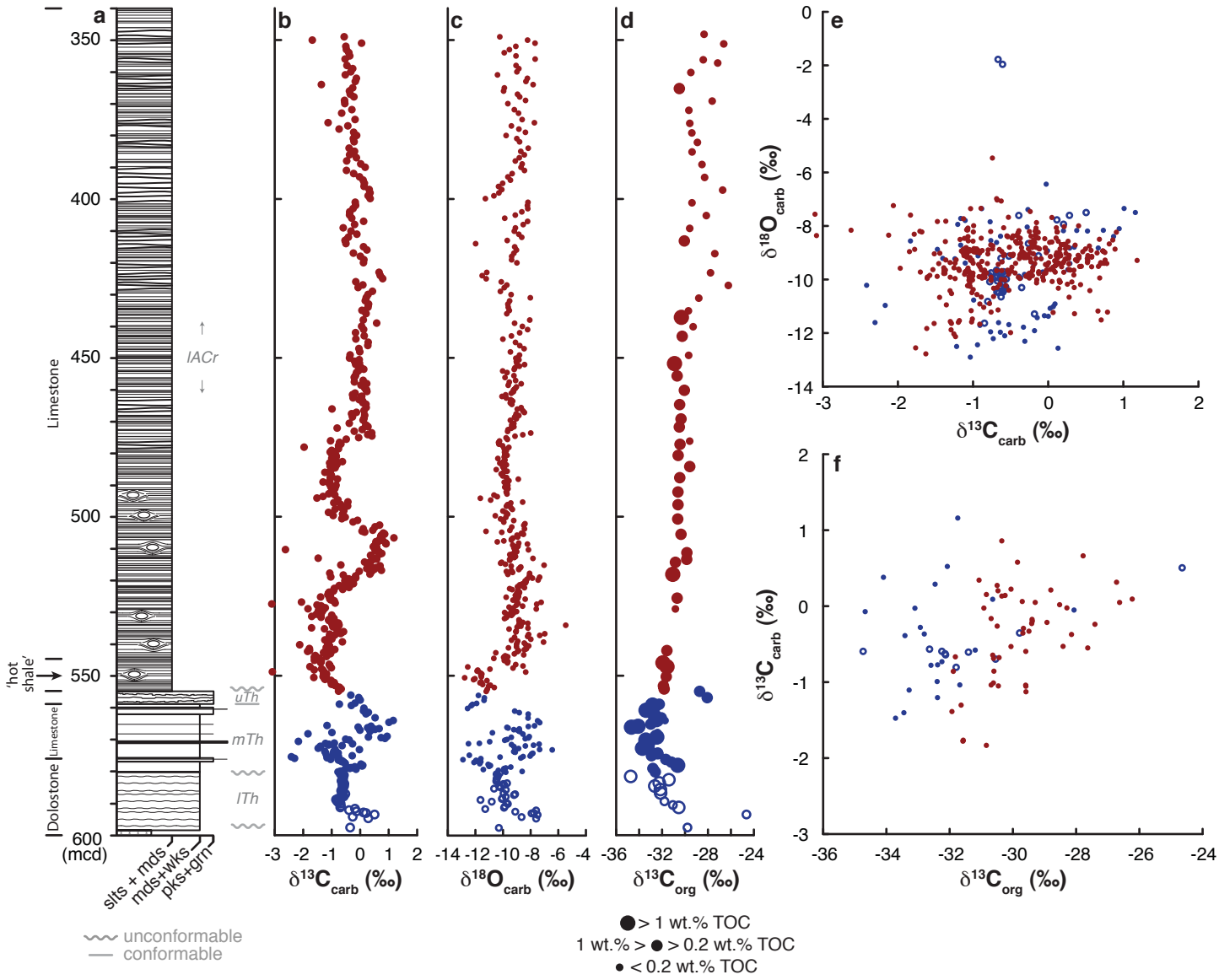

Figure 5
Click here to download Figure: NTGS Fig 5.pdf

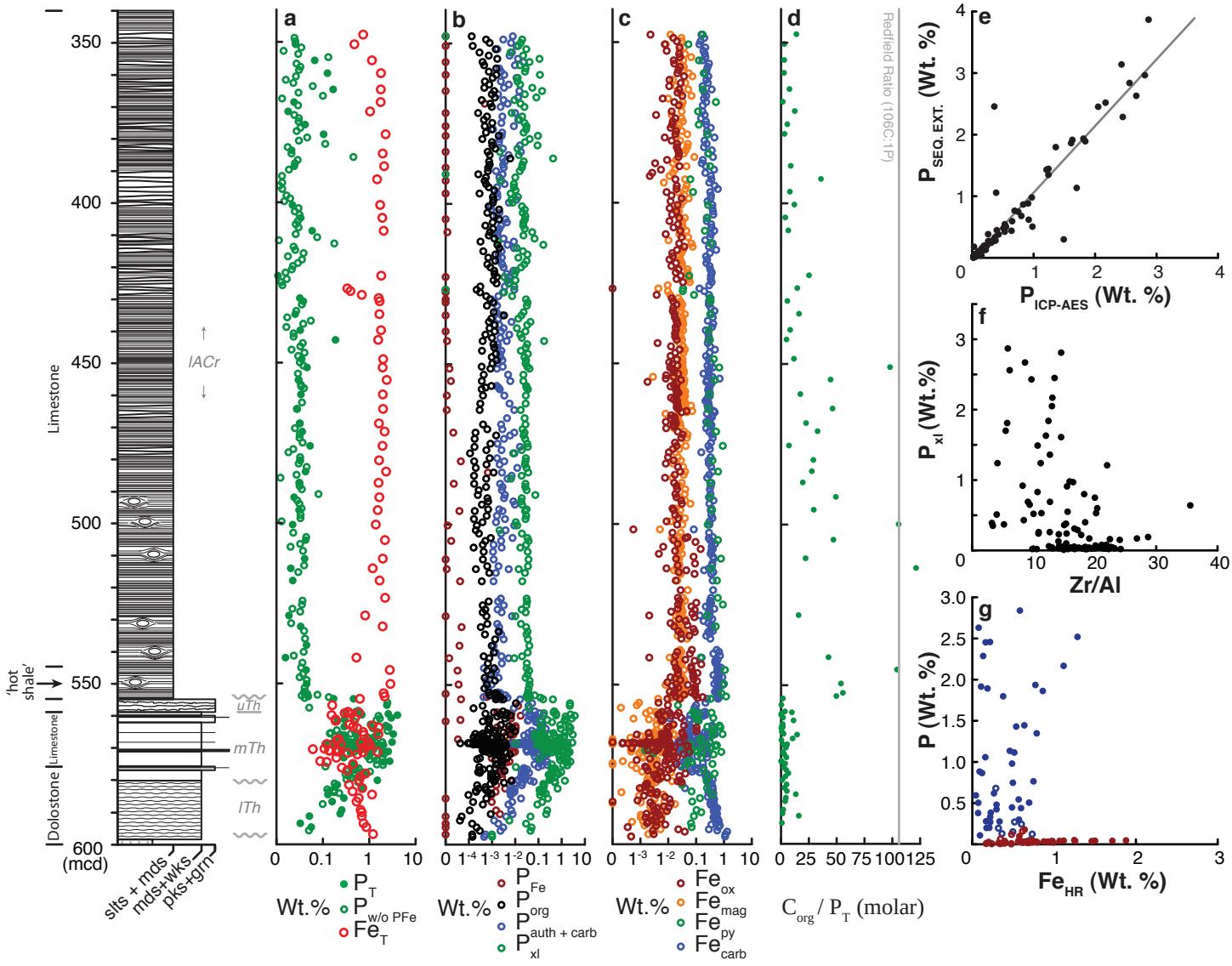

Figure 6
Click here to download Figure: NTGS Fig 6 revised.pdf

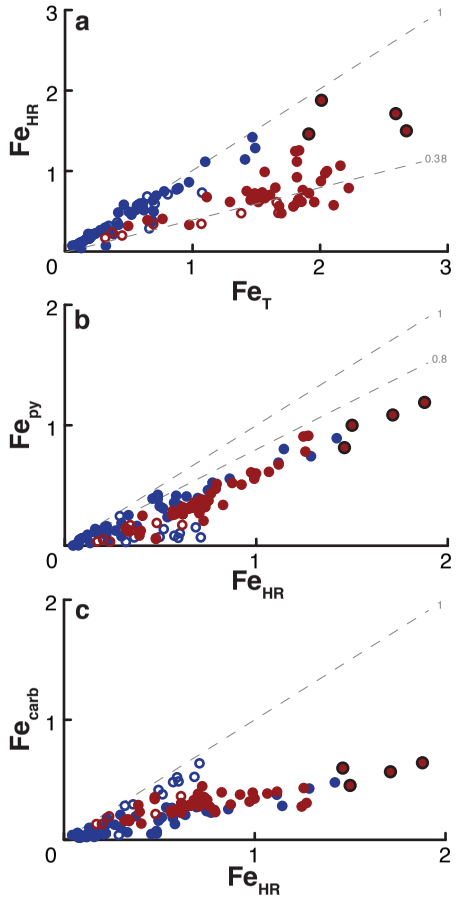

Figure 7
Click here to download Figure: NTGS Fig 7.pdf

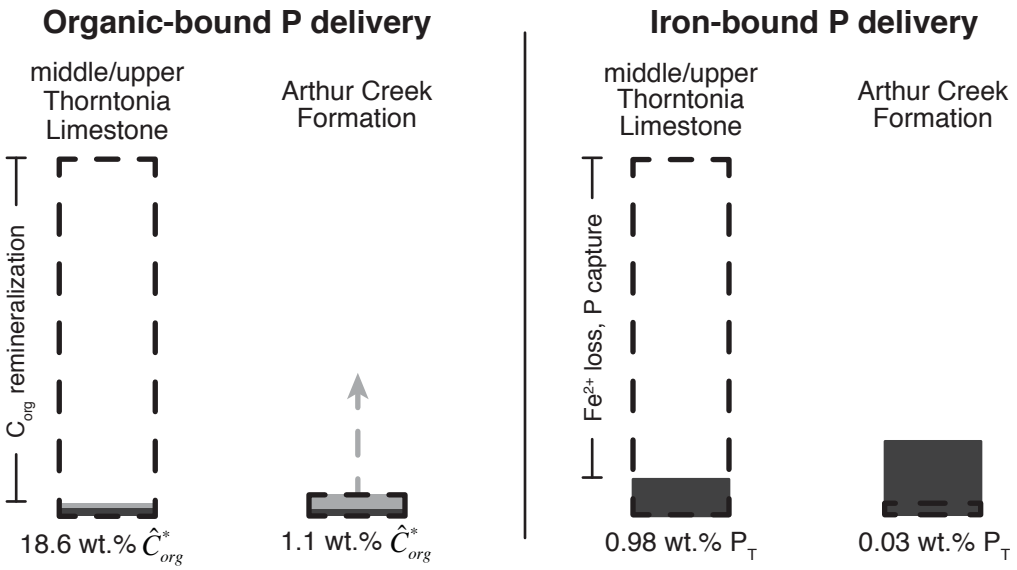

Supplementary Information

Click here to download Supplemental file: Supplementary Information for Revision 2.pdf

Supplementary Figure 1

Click here to download Supplemental file: NTGS Fig S1.pdf

Supplementary Figure 2
Click here to download Supplemental file: NTGS Fig S2.pdf

Supplementary Data Spreadsheet

Click here to download Supplemental file: NTGS Final Spreadsheet.xlsx